PI 3-kinase delta enhances axonal PIP_3 to support axon regeneration in the adult CNS

Amanda C. Barber[1,11], Rachel S. Evans[1,11], Bart Nieuwenhuis[1,10,11], Craig S. Pearson[1], Joachim Fuchs[5], Amy R. MacQueen[9], Susan van Erp[8], Barbara Haenzi[1], Lianne A. Hulshof[1], Andrew Osborne[1], Raquel Conceicao[1], Sarita S. Deshpande[1], Joshua Cave[1], Charles ffrench-Constant[8], Patrice D. Smith[7], Klaus Okkenhaug[6], Britta J. Eickholt[5], Keith R. Martin[1,3,4], James W. Fawcett[1,2] and Richard Eva[1, 12]

[1] John Van Geest Centre for Brain Repair, Department of Clinical Neurosciences, University of Cambridge, Cambridge CB2 OPY, United Kingdom.

[2] Centre of Reconstructive Neuroscience, Institute of Experimental Medicine, Czech Academy of Sciences, Prague, Czech Republic.

[3] Centre for Eye Research Australia, Royal Victorian Eye and Ear Hospital, Melbourne, VIC, Australia.

[4] Ophthalmology, Department of Surgery, University of Melbourne, Melbourne, VIC, Australia.

[5] Institute of Biochemistry, Charité - Universitätsmedizin Berlin, Charitéplatz 1, 10117, Berlin, Germany.

[6] Department of Pathology, Tennis Court Road, University of Cambridge, Cambridge, United Kingdom.

[7] Department of Neuroscience, Carleton University, Ottawa, Ontario, Canada.

[8] MRC Centre for Regenerative Medicine, University of Edinburgh, Edinburgh, United Kingdom.

[9] Laboratory of Lymphocyte Signalling and Development, Babraham Institute, Cambridge CB22 1A3.

[10] Laboratory for Regeneration of Sensorimotor Systems, Netherlands Institute for Neuroscience, Royal Netherlands Academy of Arts and Sciences (KNAW), 1105 BA Amsterdam, the Netherlands.

[11] These authors contributed equally.

[12] Corresponding author: re263@cam.ac.uk

Summary

Peripheral nervous system (PNS) neurons support axon regeneration into adulthood, whereas central nervous system (CNS) neurons lose regenerative ability after development. To better understand this decline whilst aiming to improve regeneration, we focused on phosphoinositide 3-kinase (PI3K) and its product phosphatidylinositol(3,4,5)-trisphosphate (PIP3). We found that neuronal PIP3 decreases with maturity in line with regenerative competence, firstly in the cell body and subsequently in the axon. We show that adult PNS neurons utilise two catalytic subunits of PI3K for efficient regeneration: p110α and p110δ. Overexpressing p110α in CNS neurons had no effect, however expression of p110δ restored axonal PIP3 and enhanced CNS regeneration in rat and human neurons and in transgenic mice, functioning in the same way as the hyperactivating H1047R mutation of p110α. Furthermore, viral delivery of p110δ promoted robust regeneration after optic nerve injury. These findings demonstrate a deficit of axonal PIP3 as a reason for intrinsic regeneration failure and show that native p110δ facilitates axon regeneration by functioning in a hyperactive fashion.

Keywords

Axon, axon regeneration, CNS regeneration, optic nerve, neuronal signalling, phosphoinositide 3-kinase, PI3K, p110 delta, phosphatidylinositol(3,4,5)-trisphosphate, PIP3.

Introduction

Adult central nervous system (CNS) neurons have a weak capacity for axon regeneration, meaning that injuries in the brain, spinal cord and optic nerve have devastating consequences (Curcio and Bradke, 2018; He and Jin, 2016). In most CNS neurons, regenerative capacity declines dramatically with development, both *in vitro* (Goldberg et al., 2002; Koseki et al., 2017) and *in vivo* (Kalil and Reh, 1979; Wu et al., 2007), so that regenerative ability is lost as axons mature. Conversely, peripheral nervous system (PNS) neurons maintain regenerative potential through adult life. This is partly because PNS neurons mount an injury response in the cell body (Puttagunta et al., 2014; Richardson et al., 1984; Richardson et al., 2009; Smith and Skene, 1997; Ylera et al., 2009), and partly because PNS axons support efficient transport of growth promoting receptors, whilst transport of these is developmentally downregulated in CNS axons (Andrews et al., 2016; Franssen et al., 2015; Gardiner et al., 2007; Hollis et al., 2009a; Hollis et al., 2009b). Studies into intrinsic regenerative capacity have implicated signalling molecules, transcription factors, epigenetic regulators, RNA binding proteins, and axon transport pathways as critical regeneration determinants (Blackmore et al., 2012; Eva et al., 2017; Fagoe et al., 2015; Hervera et al., 2019; Park et al., 2008; Tedeschi and Bradke, 2017; Weng et al., 2018; Zhang et al., 2019). This leads to a model where axon growth capacity is controlled by genetic and signalling events in the cell body, and by the selective transport of growth machinery into the axon to facilitate re-establishment of a growth cone after injury.

In order to better understand the mechanisms regulating axon regeneration from within the axon and the cell body, we focused on the class I phosphoinositide 3-kinases (PI3Ks). These enzymes mediate signalling through integrins, growth factor and cytokine receptors, by producing the membrane phospholipid PIP3 from PIP2 (phosphatidylinositol(3,4,5)-trisphosphate from phosphatidylinositol(4,5)-bisphosphate). Class 1 PI3Ks comprise 4 catalytic isoforms, called p110α, β, γ and δ, with distinct roles for some of these emerging in

specific cell populations and signal transduction scenarios (Bilanges et al., 2019). The p110α and p110β isoforms are ubiquitously expressed, whilst p110δ and p110γ are highly enriched in all leukocyte subtypes (Hawkins and Stephens, 2015). Interestingly, p110δ is also expressed in selected neuronal populations and microglia (Eickholt et al., 2007; Low et al., 2014; Martinez-Marmol et al., 2019).

The class I phospholipids are strongly implicated in the regulation of regenerative ability because transgenic deletion of PTEN, an enzyme which opposes PI3K by converting PIP3 back to PIP2, promotes CNS regeneration (Geoffroy et al., 2015; Liu et al., 2010; Park et al., 2008; Willenberg et al., 2016). Whilst PTEN acts on the lipids of all class I PI3Ks, the contribution of the individual PI3K isoforms to neuronal function remains largely unknown. p110δ has been shown to be required for the efficient regeneration of dorsal root ganglion (DRG) neurons in the PNS (Eickholt et al., 2007) and p110α mediates olfactory bulb axon growth during chick development (Hu et al., 2013) whilst p110β and p110γ have not been studied in the context of axon growth.

The data on PTEN loss indicate a pro-regenerative role for PIP3, in keeping with other studies that implicate PI3K in the regulation of axon growth and regeneration (Al-Ali et al., 2017; Cosker and Eickholt, 2007). Importantly, PTEN deletion enhances regeneration through downstream signalling within the cell body (Park et al., 2008), but it is not known whether it also has effects within the axon. PIP3 may be required at the growth cone for a number of functions, including regulation of cytoskeletal dynamics, response to guidance cues and trafficking of receptors to the surface membrane (Eva et al., 2010; Henle et al., 2011; Kakumoto and Nakata, 2013; Kath et al., 2018; Lindsay and McCaffrey, 2004; Ming et al., 1999; Tsujita and Itoh, 2015). Highly localised PI3K activity in the tip of developing hippocampal axons is essential for the establishment of polarity (Menager et al., 2004; Shi et al., 2003), whilst spatially segregated PI3K activity is required at the growth cone of PNS axons to elicit rapid

axon growth (Zhou et al., 2004), such as occurs during PNS axon regeneration (Smith and Skene, 1997). We reasoned that adult CNS regenerative failure might be associated with a decline in PIP3 within the axon, and wondered whether specific PI3K isoforms were required for efficient axonal PIP3 production to support regeneration.

We investigated the role of class I PI3K isoforms in DRG axon regeneration, and found that both p110α and p110δ are required for growth cone redevelopment, but that p110δ is specifically required within the axon. In rat cortical neurons we found PIP3 to be sharply downregulated with development, firstly in the cell body, then diminishing in the axon at the time when regenerative ability also declines. We attempted to restore PIP3 through overexpression of either p110α or p110δ, however only p110δ led to elevated axonal PIP3. Importantly, by introducing the hyperactivating H1047R mutation into p110α we found that it could mimic the effect of p110δ, with expression of either facilitating axon regeneration of rat and human CNS neurons *in vitro*. Furthermore, transgenic expression of p110δ or p110α^{H1047R} in adult retinal ganglion cell (RGC) neurons led to enhanced survival and axon regeneration after optic nerve crush, whilst viral delivery of exogenous p110δ further enhanced regeneration, demonstrating the potential for translational development. Importantly, overexpression of p110δ has both somatic and axonal effects, also signalling through S6 ribosomal protein in the cell body. These findings demonstrate a deficit of axonal PIP3 as a novel reason for intrinsic regenerative failure, whilst establishing that native p110δ functions like p110α^{H1047R} to enable CNS axon regeneration. This evidence of innate hyperactivity has important implications for understanding the role of p110δ in other cell types, such as T- and B-cells. Our results emphasize the importance of elevating growth-promoting pathways in the axon as well as the cell body, in order to stimulate axon regeneration.

Results

Gene expression of p110 isoforms in the nervous system

Because localised axonal activation of PI3K is essential for rapid PNS axon growth (Zhou et al., 2004), we reasoned that there may be specific PI3K isoforms that support regeneration within PNS axons, and that these might be under-represented in CNS neurons. p110δ is expressed in DRG neurons where it plays a role in axon regeneration (Eickholt et al., 2007), however the contribution of other PI3K isoforms has not been examined. We first investigated the RNA expression of the individual p110 subunits (p110α, β, γ and δ) in four published neuronal RNAseq datasets (Figure S1, after the references section), examining expression in DRG neurons during axon growth and regeneration (Tedeschi et al., 2016), in cortical neurons developing *in vitro* (Koseki et al., 2017) and in the Brain-RNAseq databases (http://www.brainrnaseq.org/) of individual cell types in mouse and human brain (Zhang et al., 2014; Zhang et al., 2016). In DRG neurons p110α, β and δ are expressed at all stages *in vitro*, whilst p110γ is expressed at very low levels. p110α is present at the highest levels, whilst p110δ is upregulated in development, and further upregulated upon peripheral nerve lesion (Figure S1A - C). In developing cortical neurons, p110α is again expressed at the highest levels, p110β and δ are present but not abundant, and p110γ is at very low levels. Remarkably, p110α, β and δ are all downregulated as cortical neurons mature (Figure S1D and E). The Brain-RNAseq database indicates p110α and β are the principal neuronal PI3K isoforms in both the mouse and human adult brain, with p110α again expressed at the highest levels, whilst p110δ and γ are enriched in microglia and macrophages, in keeping with their predominant expression in white blood cells (Figure S1F - M). Collectively, these datasets indicate that p110α, β and δ are expressed in regenerative sensory neurons, but are almost absent or downregulated with maturation in CNS neurons. We therefore chose to investigate the contribution of the p110α, β and δ isoforms of PI3K to axon regeneration of DRG neurons.

p110α and δ are required for DRG axon regeneration

We used laser axotomy to sever the axons of adult DRG neurons and measured the effect of specific inhibitors of the p110α, β and δ isoforms on the rate of growth cone regeneration (Figure 1). Inhibiting either p110α or δ reduced the rate of regeneration, as did pan-PI3K inhibition (α, β and δ) or targeting p110α and δ together. Inhibiting p110β had no effect on the rate of regeneration, but inhibiting all of the isoforms increased the time taken to develop a new growth cone (Figure 1A and B). Some inhibitors also caused uncut axons to stop growing, so we measured the extension rate of uncut axons in the same field of view. Treatment with p110α inhibitors, pan-PI3K or dual α / δ inhibitors led to a dramatic reduction in the percentage of uncut axons extending in the two-hour period, whilst they continued to extend in the presence of specific p110δ inhibitors (Figure 1C and D). We next examined the effect of PI3K inhibition using microfluidic compartmentalised chambers, in which axons extend through microchannels into a separate compartment from the cell bodies (Figure 1E). Inhibition of p110α or p110δ showed different effects depending on localization. Inhibition of p110δ in the axonal compartment reduced the percentage of regenerating axons, but had no effect in the somatic chamber. In contrast, the p110α inhibitor A66 reduced regeneration when applied either to the axonal or somatic compartment, and also increased the time taken to generate a new growth cone (Figure 1F). These data show that DRG neurons require p110α and δ for efficient regeneration. Axon growth and regeneration requires p110α activity in both the cell body and axon, whilst axon regeneration further relies on p110δ activity specifically within the axon.

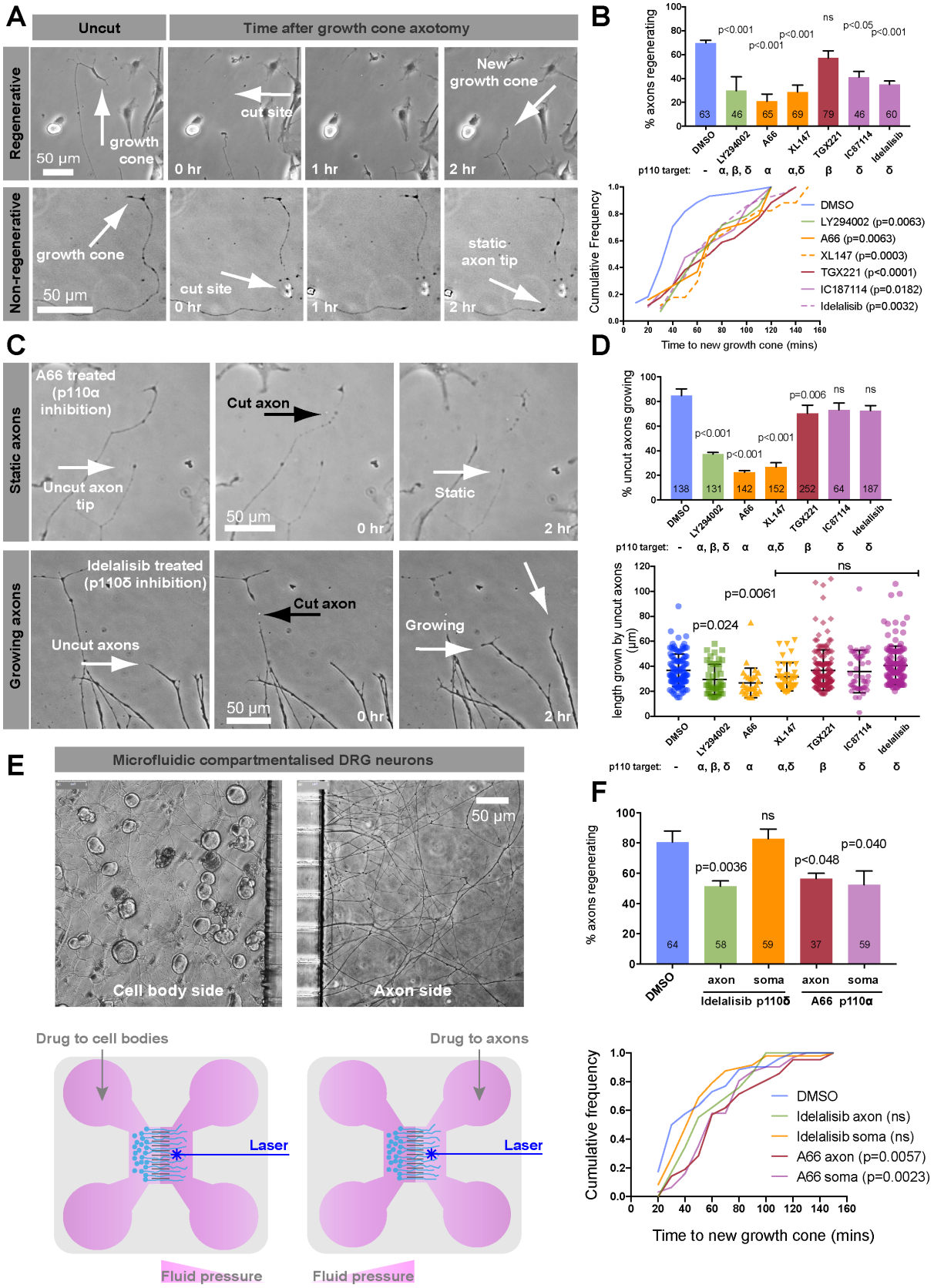
A
Uncut
Time after growth cone axotomy
Regenerative
Non-regenerative
growth cone
50 µm
cut site
0 hr
1 hr
New growth cone
2 hr
static axon tip
B
% axons regenerating
p<0.001
p<0.001
p<0.001
ns
p<0.05
p<0.001
63
46
65
69
79
46
60
DMSO
LY294002
A66
XL147
TGX221
IC87114
Idelalisib
p110 target: - α, β, δ α α,δ β δ δ
Cumulative Frequency
DMSO
LY294002 (p=0.0063)
A66 (p=0.0063)
XL147 (p=0.0003)
TGX221 (p<0.0001)
IC187114 (p=0.0182)
Idelalisib (p=0.0032)
Time to new growth cone (mins)
C
Static axons
Growing axons
A66 treated (p110α inhibition)
Uncut axon tip
Cut axon
Static
Idelalisib treated (p110δ inhibition)
Uncut axons
Growing
D
% uncut axons growing
p<0.001
p<0.001
p<0.001
p=0.006
ns
ns
138
131
142
152
252
64
187
length grown by uncut axons (µm)
p=0.0061
p=0.024
ns
E
Microfluidic compartmentalised DRG neurons
Cell body side
Axon side
Drug to cell bodies
Drug to axons
Laser
Fluid pressure
F
% axons regenerating
p=0.0036
ns
p<0.048
p=0.040
64
58
59
37
59
axon
soma
axon
soma
Idelalisib p110δ
A66 p110α
Cumulative frequency
DMSO
Idelalisib axon (ns)
Idelalisib soma (ns)
A66 axon (p=0.0057)
A66 soma (p=0.0023)
Time to new growth cone (mins)

Figure 1.

Figure 1. p110α and δ are required for DRG axon regeneration; p110δ functions in the axonal compartment

See also supplemental figure S1.

(A) Laser injured DRG axons showing growth cone regeneration (upper panels) and regenerative failure (lower panels). Arrows as indicated.

(B) Percentage of regenerating axons of DIV 1-2 adult DRG neurons in the presence of p110 inhibitors, 2 h after injury. Numbers on bars are injured axons per group. The lower graph is time taken to growth cone development. Error bars are s.e.m. P values indicate statistical significance analysed by Fishers exact (upper graph) or Kruskal-Wallis test (lower graph).

(C) Examples of static vs. growing uninjured axons treated with p110α or δ inhibitors as indicated.

(D) Percentage of uninjured, growing axons in the presence of p110 inhibitors. Numbers on bars are uncut axons analysed. Lower graph shows length grown in 2 h. Error bars are s.e.m. P values indicate significance measured by Fishers exact test (upper graph) or ANOVA with Tukey's post-hoc analysis (lower graph).

(E) Adult DRG neurons in microfluidic compartmental chambers. Cell bodies on the left side, axons extending through microchannels on the right. Lower panels are schematics.

(F) Percentage of regenerating axons in microfluidic chambers. p110α or δ inhibitors were applied to either soma or axons. Lower graph is time to formation of a growth cone. Error bars are s.e.m. P values indicate statistical significance as measured by Fishers exact test (upper graph) or by Kruskal-Wallis test (lower graph).

PIP3 is developmentally downregulated in cortical neurons

The RNAseq data described above (Figure S1) suggest that PI3K expression increases with maturation in DRG neurons whilst it is downregulated as cortical neurons mature. CNS regenerative failure might therefore be due to insufficient PI3K activity within the axon, and insufficient PIP3. PIP3 is implicated in numerous aspects of axon growth but its developmental distribution has not been examined. PIP3 has previously been localised using fluorescently tagged pleckstrin homology (PH)-domain reporters, such as AKT-PH-GFP, however the principle readout of these reporters is translocation to the surface membrane, and they do not report on abundance or "steady state" distribution. In order to accurately measure PIP3 in neurons developing *in vitro* we optimised a fixation technique (Hammond et al., 2009),

developed for antibody-based PIP3 detection on immobilised membrane phospholipids utilising a PIP3 antibody widely used for biochemical assays. To validate this method in neurons, we isolated DRG neurons from transgenic mice expressing AKT-PH-GFP at low levels (Nishio et al., 2007) to avoid inhibition of downstream signalling (Varnai et al., 2005). Live imaging of adult DRG neurons from these mice revealed dynamic hotpots of PIP3 at the axon growth cone (Figure S2A and Movie 1), and membrane labelling confirmed these hotspots are not regions of membrane enrichment (Figure S2B and Movie 2). Phospholipid fixation and labelling with anti-PIP3 revealed colocalization between AKT-PH-GFP and anti-PIP3 at regions within DRG growth cones (Figure S2C), as well as at hotspots and signalling platforms in non-neuronal cells from DRG cultures (Figure S2D). In addition to validating this technique, our data also confirm the presence of dynamic PIP3 in the growth cone of regenerative DRG neurons. To further confirm the specificity of the stain for PIP3 we stimulated N1E cells with insulin and labelled for PIP3 in the presence or absence of the pan-PI3K inhibitor GDC-0941, detecting increased PIP3 staining after insulin stimulation alone, and not in the presence of the PI3K inhibitor (Figure S2 E, F and G).

We then labelled E18 cortical neurons at 3, 8 and 16 days *in vitro* (DIV) to detect endogenous PIP3. At DIV 3 we detected high levels of PIP3 in the cell body, and particularly in the distal axon and growth cone (Figure 2A, D and E). By DIV 8 there was a sharp decline in PIP3 at the cell body (Figure 2B and D), but only a small decrease in growth cone PIP3 (Figure 2B and E), indicating that during the period of rapid axon extension, neurons possess high levels of PIP3 in axonal growth cones. At DIV 16, cortical neurons exhibit a sharp decline in regenerative ability (Koseki et al., 2017). At this stage, we detected markedly reduced levels of PIP3 at the growth cone while they remained low at the cell body (Figure 2C, D and E). This indicates a global reduction in PIP3 as cortical neurons develop and demonstrates that the loss of regenerative ability coincides with a deficiency in axonal PIP3 production.

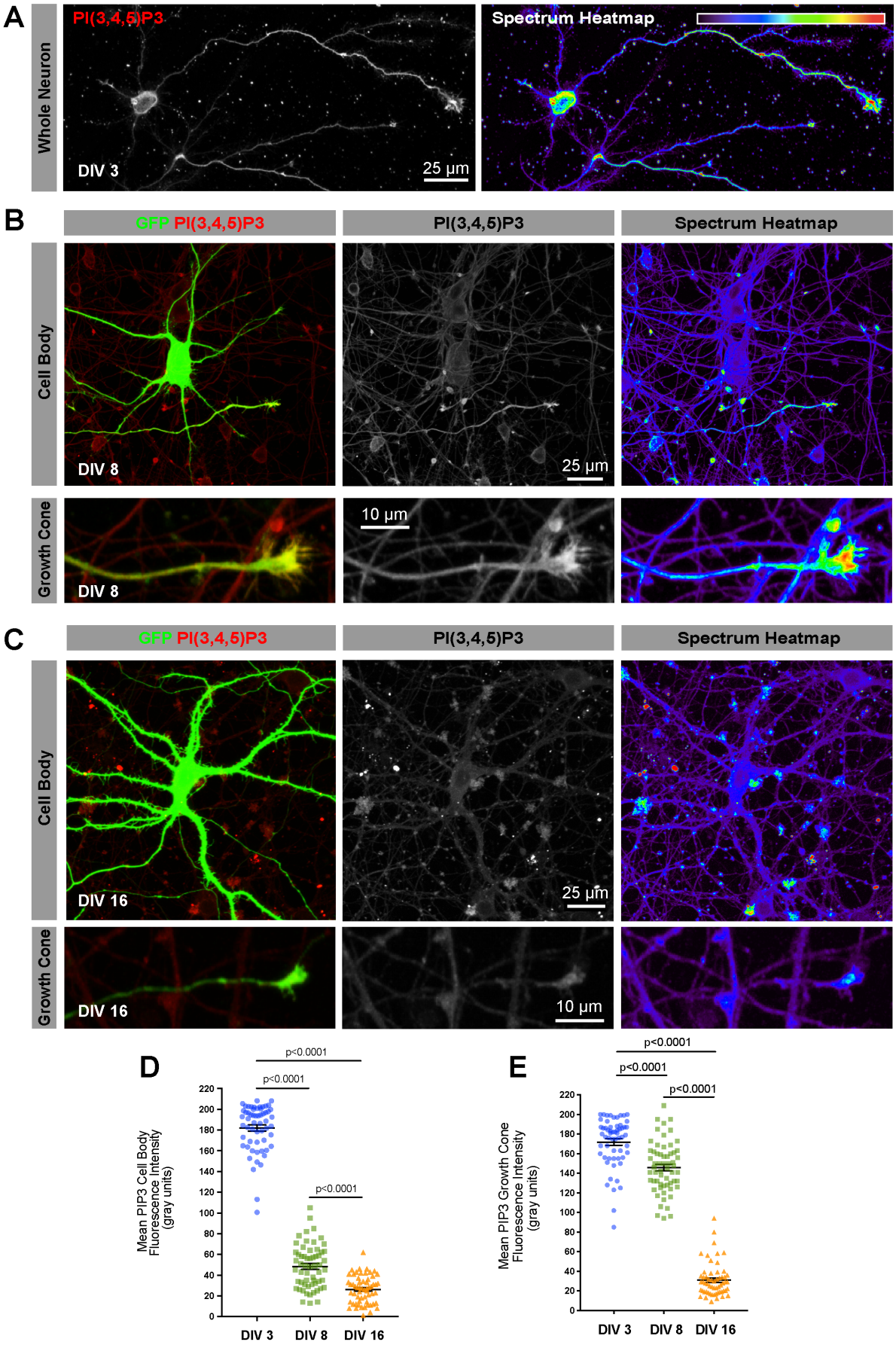
A
Whole Neuron
PI(3,4,5)P3
DIV 3
25 µm
Spectrum Heatmap
B
GFP PI(3,4,5)P3
PI(3,4,5)P3
Spectrum Heatmap
Cell Body
DIV 8
25 µm
Growth Cone
DIV 8
10 µm
C
GFP PI(3,4,5)P3
PI(3,4,5)P3
Spectrum Heatmap
Cell Body
DIV 16
25 µm
Growth Cone
DIV 16
10 µm
D
Mean PIP3 Cell Body Fluorescence Intensity (gray units)
p<0.0001
p<0.0001
p<0.0001
DIV 3
DIV 8
DIV 16
E
Mean PIP3 Growth Cone Fluorescence Intensity (gray units)
p<0.0001
p<0.0001
p<0.0001
DIV 3
DIV 8
DIV 16

Figure 2.

Figure 2. PIP3 is developmentally downregulated in cortical neurons maturing *in vitro*, first in the soma, then at the growth cone.

See also supplemental figure S2 and Movies 1 and 2.

(A) DIV 3 cortical neurons immunolabelled for PIP3.

(B) DIV 8 cortical neuron transfected with GFP and immunolabelled for PIP3.

(C) DIV 16 cortical neuron transfected GFP and immunolabelled for PIP3.

(D) Somatic PIP3 quantification in the soma at increasing days *in vitro*. Error bars are s.e.m. P values are significance measured by ANOVA with Tukey's post-hoc analysis.

(E) Growth cone PIP3 quantification at increasing days *in vitro*. Error bars are s.e.m. P values indicate significance measured by ANOVA with Tukey's post-hoc analysis.

Expression of p110δ or p110α^{H1047R} elevates PIP3 in the soma and axon

The results above show that PI3K and PIP3 are developmentally downregulated in CNS axons as they lose their regenerative ability. In DRG neurons, which continue to express PI3K and produce PIP3, the p110α and δ isoforms are necessary for efficient axon regeneration (Figure 1). We therefore asked whether we could increase PIP3 levels and restore regeneration to CNS neurons by ectopic expression of p110α, its hyperactive H1047R variant p110α^{H1047R} (Mandelker et al., 2009) or p110δ. Previous work has shown that p110δ and p110α^{H1047R} can sustain downstream AKT activation upon overexpression in fibroblasts, acting independently of active Ras, whilst native p110α does not (Kang et al., 2006). These PI3Ks were expressed in cortical neurons at DIV 16, and PIP3 was measured by quantitative immunofluorescence. We used dual-promoter constructs expressing untagged p110 and GFP, in order to avoid potential interference of PI3K function by a protein tag.

Compared with cells expressing GFP alone, expression of p110α had no effect on PIP3 levels in DIV 16 neurons, either in the cell body or within the axons (Figure 3 A, B,C and D). In contrast, overexpression of either p110α^{H1047R} or p110δ led to a small but significant increase in PIP3 in the cell body (Figure 3, A and C), and a striking increase in PIP3 at axon growth

cones (Figure 3, B and D). These findings indicate that p110δ and p110α^{H1047R} function in a hyperactive fashion to generate PIP3 in cortical neurons, with the strongest effect in growth cones.

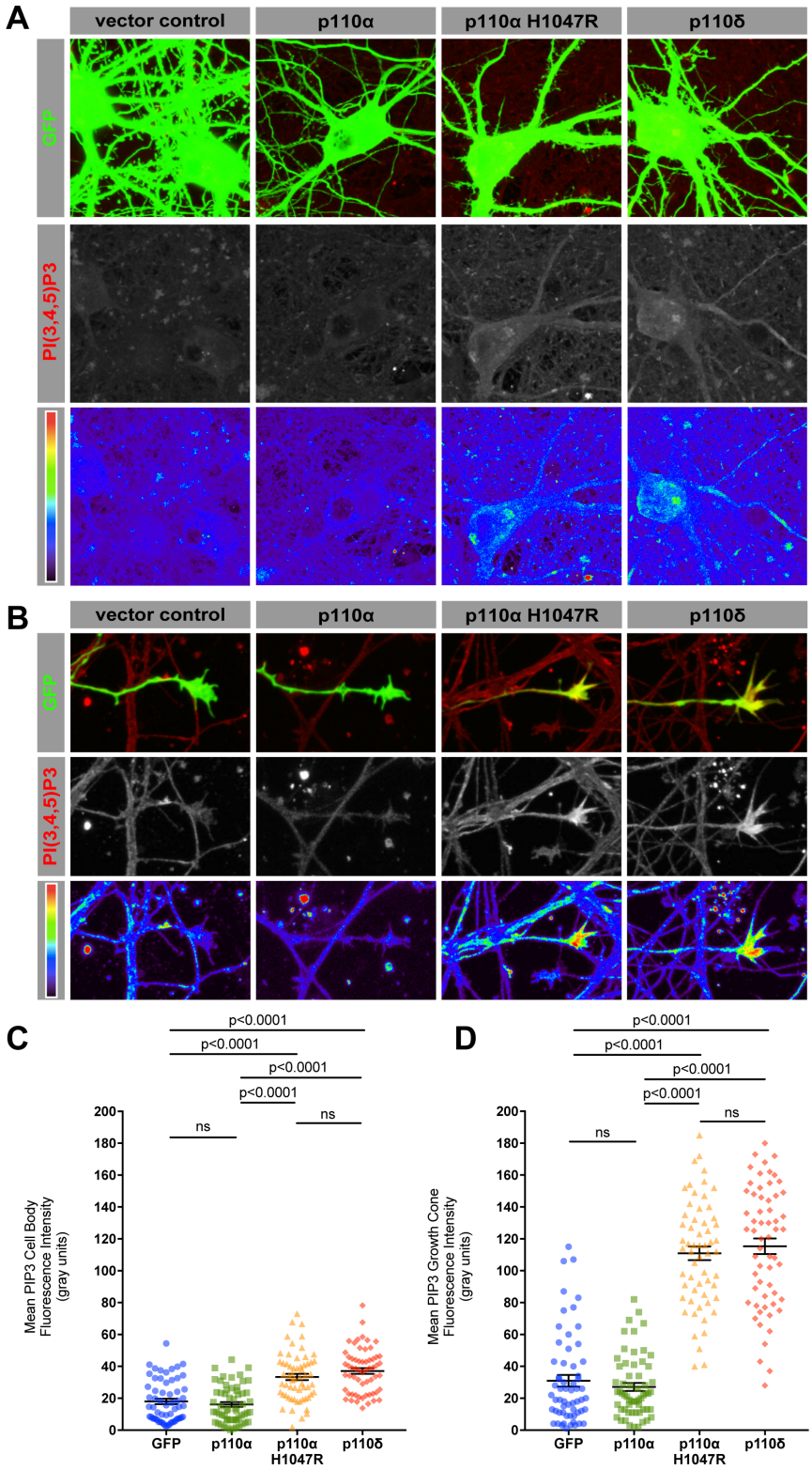

Figure 3.

Figure 3. p110δ or p110α^{H1047R} expression elevates PIP3 in the soma and axon, whilst native p110α does not

(A) PIP3 immunofluorescence in the soma of DIV 16 cortical neurons expressing p110 isoforms and GFP. Spectrum heatmap shows fluorescence intensity.

(B) PIP3 immunofluorescence at the axonal growth cone of DIV 16 neurons expressing p110 isoforms and GFP. Spectrum heatmap shows fluorescence intensity.

(C) Quantification of PIP3 immunofluorescence in the soma. Error bars are s.e.m. P values indicate significance as measured by ANOVA with Tukey's post-hoc analysis.

(D) Graph showing PIP3 quantification of immunofluorescence at the axon growth cone. Error bars are s.e.m. P values indicate significance measured by ANOVA with Tukey's post-hoc analysis.

Expression of p110δ or p110α^{H1047R} increases axon and dendrite growth

We next investigated the effect of p110δ, p110α or p110α^{H1047R} overexpression on the regulation of axon growth in cortical neurons developing *in vitro*. Expression of either p110δ or p110α^{H1047R} at DIV 2 led to a moderate increase in axon length by DIV 4, compared with neurons expressing either GFP alone or native p110α (Figure 4A and B). p110δ or p110α^{H1047R} expression also led to a small increase in the dendrite length (Figure 4A and C). This led to an increase in axon/dendrite length ratio, with axons approximately 31.5 times longer than dendrites, while control neurons have axons 21.8 times longer than dendrites. None of the PI3K isoforms therefore affected neuronal polarisation (Figure 4A and D). We also examined the effects of PI3K overexpression on dendrite length and branching at a later developmental stage (transfecting at DIV 10, and analysing at DIV 14). Again, p110δ and p110α^{H1047R} behaved similarly, expression of either construct leading to statistically significant increases in both the number of dendrite branches and the total dendrite length, compared with control-transfected neurons. In contrast, expression of native p110α had no effect (Figure 4E, F and G). The PI3K pathway is a well know regulator of cell size, so we also measured hypertrophy. Overexpression of either p110δ or p110α^{H1047R} led to an increase in cell body size, compared with either GFP or p110α (Figure 4H). To confirm downstream signalling through the PI3K

pathway, we employed phosphorylation-specific immunolabelling of ribosomal S6 protein, a transcriptional regulator routinely used as a reporter of somatic signalling through the PI3K/AKT/mTOR pathway. p110δ or p110α^{H1047R} expression led to a strong phospho-S6 signal compared with GFP expressing controls, whilst expression of p110α again had no effect (Figure 4E and I). These findings confirm that hyperactive p110α^{H1047R} behaves like p110δ to trigger downstream signalling through the PI3K pathway in neuronal soma, with effects on size, dendrite branching and axon length. The results demonstrate that p110δ and p110α^{H1047R} enhance both axonal and dendritic growth whilst native p110α does not.

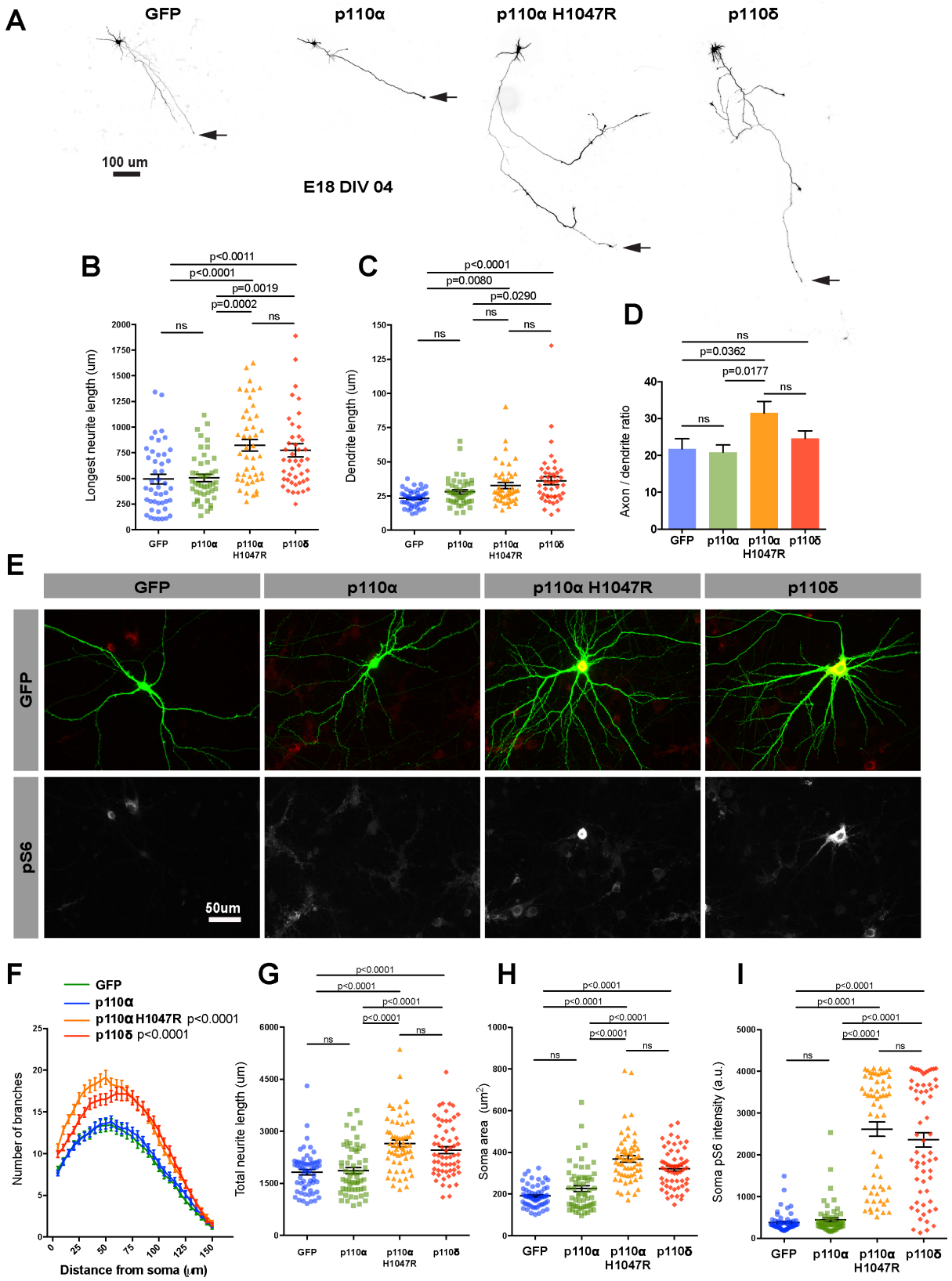
A
GFP
p110α
p110α H1047R
p110δ
100 um
E18 DIV 04
B
Longest neurite length (um)
p<0.0011
p<0.0001
p=0.0019
p=0.0002
ns
ns
GFP
p110α
p110α H1047R
p110δ
C
Dendrite length (um)
p<0.0001
p=0.0080
p=0.0290
ns
ns
ns
D
Axon / dendrite ratio
ns
p=0.0362
p=0.0177
ns
ns
E
GFP
p110α
p110α H1047R
p110δ
pS6
50um
F
GFP
p110α
p110α H1047R p<0.0001
p110δ p<0.0001
Number of branches
Distance from soma (μm)
G
Total neurite length (um)
p<0.0001
p<0.0001
p<0.0001
p<0.0001
ns
ns
H
Soma area (um²)
p<0.0001
p<0.0001
p<0.0001
p<0.0001
ns
ns
I
Soma pS6 intensity (a.u.)
p<0.0001
p<0.0001
p<0.0001
p<0.0001
ns
ns

Figure 4.

Figure 4. Expression of p110δ or p110α^{H1047R} increases axon and dendrite growth of cortical neurons developing *in vitro*, whilst native p110α does not

(A) DIV 4 cortical neurons expressing p110 isoforms and GFP. Arrow marks the axon tip.

(B) Quantification of axon length. n = 45 neurons per group. Error bars are s.e.m. P values indicate significance measured by ANOVA with Tukey's post-hoc analysis.

(C) Quantification of dendrite length. n = 45 neurons per group. Error bars are s.e.m. P values indicate significance measured by ANOVA with Tukey's post-hoc analysis.

(D) Quantification of the axon:dendrite length ratio. n = 45 neurons per group. Error bars are s.e.m. P values indicate significance measured by ANOVA with Tukey's post-hoc analysis.

(E) DIV 14 cortical neurons expressing p110 isoforms and GFP, immunolabelled for pS6.

(F) Sholl analysis of branches. n = 60 neurons per group. Error bars are s.e.m. P values indicate significance measured by repeated measure ANOVA with Bonferonni's post-hoc test.

(G) Quantification of the total neurite length. n = 60 neurons per group. Error bars are s.e.m. P values indicate significance measured by ANOVA with Tukey's post-hoc analysis.

(H) Quantification of soma area. n = 60 neurons per group. Error bars are s.e.m. P values indicate significance measured by ANOVA with Tukey's post-hoc analysis.

(I) Quantification of the pS6 immunofluorescence. n = 60 neurons per group. Error bars are s.e.m. P values indicate significance measured by ANOVA with Tukey's post-hoc analysis.

p110δ and p110α^{H1047R} promote axon regeneration of CNS neurons *in vitro*

To determine whether activation of p110 can facilitate CNS regeneration we first examined the effects of overexpression on axon regeneration of cortical neurons using an *in vitro* model of mature CNS regeneration, comparing overexpression of either p110δ, p110α or p110α^{H1047R}. In this model, axon regeneration ability is progressively lost with maturity, and molecules that promote regeneration may differ from those that promote developmental outgrowth (Koseki et al., 2017). *In vitro* laser axotomy was used to sever the axons of E18 cortical neurons cultured to DIV 15-18, at which stage cortical neurons have a limited capacity for regeneration (Eva et al., 2017; Koseki et al., 2017). Expression of either p110δ or p110α^{H1047R} led to a sharp increase in the percentage of axons regenerating after axotomy compared with GFP expressing controls (rising from 16% for control neurons to 61% for p110α^{H1047R} expressors, and 57% for cells

expressing p110δ). p110α expression again had no effect (Figure 5A and B and Movies 3 and 4). Expression of p110δ or p110α^{H1047R} also led to an increase in the length of regenerated axons, and a trend towards shorter time of onset to regeneration compared to controls (Figure 5 C and D).

We further investigated the translational potential of p110δ by examining axon regeneration in human neurons maturing *in vitro* (human embryonic stem cells (hESC)). We have previously demonstrated that these lose their regenerative ability *in vitro* when cultured beyond 50 days (Koseki et al., 2017). We found that overexpression of p110δ fully restored the regenerative ability to a level observed for younger neurons (Figure 5E and F). We observed no difference in the length of regenerated axons compared with GFP-expressing control neurons (Figure 5G), but there was a tendency for p110δ expressing neurons to initiate regeneration faster (Figure 5H). Overexpression of p110δ therefore enables CNS axon regeneration in both rat and human neurons, and this is mimicked by hyperactive p110α^{H1047R}. We therefore proceeded to test whether PI3K expression could facilitate axon regeneration in the adult CNS *in vivo*.

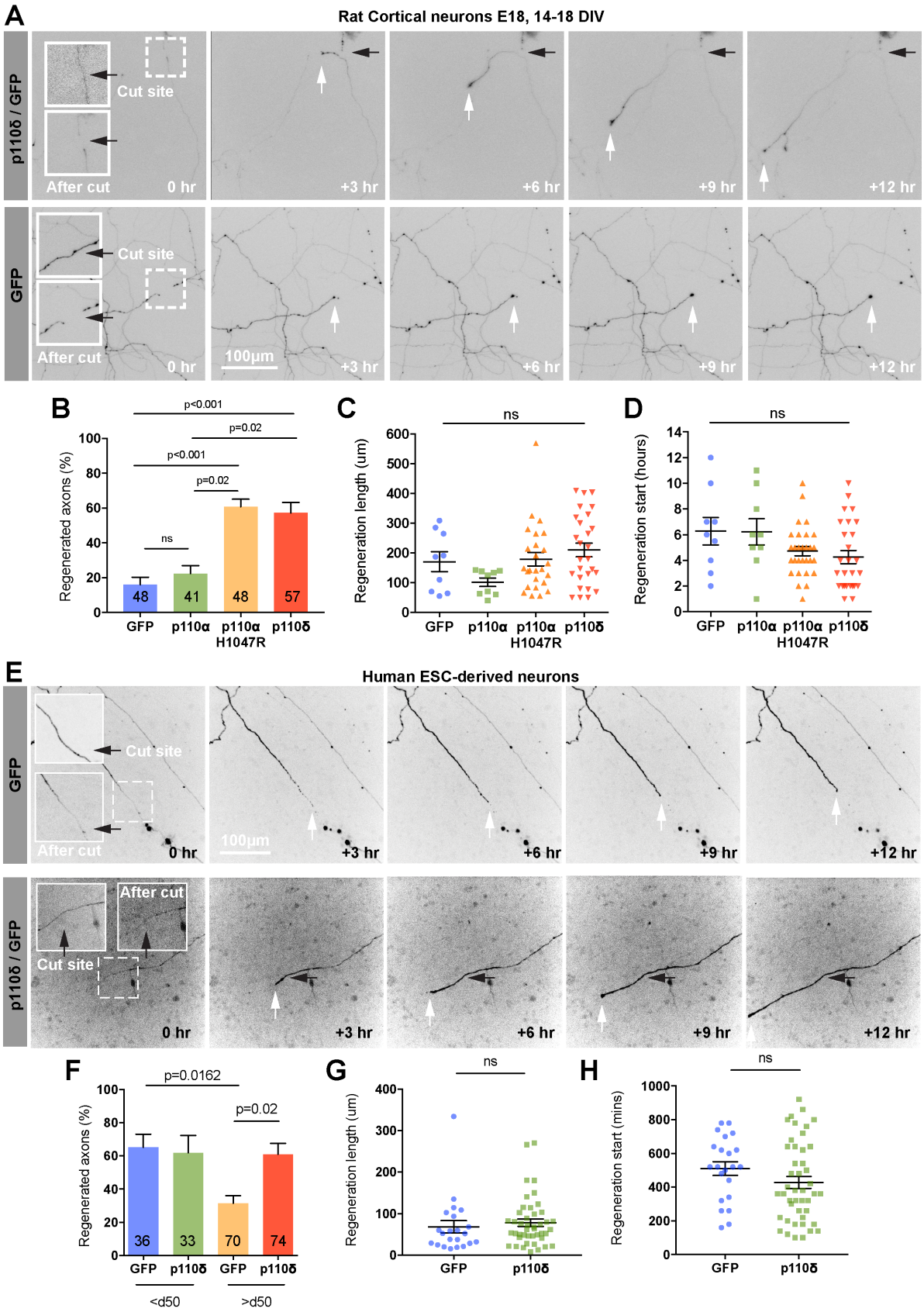
A
Rat Cortical neurons E18, 14-18 DIV
p110δ / GFP
GFP
Cut site
After cut
0 hr
+3 hr
+6 hr
+9 hr
+12 hr
100µm
B
Regenerated axons (%)
p<0.001
p=0.02
p<0.001
p=0.02
ns
48
41
48
57
GFP
p110α
p110α H1047R
p110δ
C
Regeneration length (um)
ns
D
Regeneration start (hours)
ns
E
Human ESC-derived neurons
F
Regenerated axons (%)
p=0.0162
p=0.02
36
33
70
74
<d50
>d50
G
Regeneration length (um)
ns
H
Regeneration start (mins)
ns

Figure 5.

Figure 5. p110δ and p110α^{H1047R} promote axon regeneration of CNS neurons *in vitro*

(A) Axotomised DIV 14-16 cortical neurons expressing p110δ and GFP or GFP alone. Axons were cut >1000 µm from the soma imaged for 14 h. Black arrows mark the cut site, white arrows marks the axon tip. See also supplemental Movies 3 and 4.

(B) Percentage of regenerating axons 14 h after laser axotomy. Numbers on bars are injured axons per group. Error bars are s.e.m. P values indicate significance measured by ANOVA with Tukey's post-hoc analysis.

(C) Quantification of axon regeneration length 14 h post-axotomy. Error bars are s.e.m. data were analysed by ANOVA with Tukey's post-hoc test.

(D) Quantification of time to start of regeneration. Error bars are s.e.m. Data were analysed by ANOVA with Tukey's post-hoc test.

(E) Axotomised human embryonic stem cell neurons p110δ and GFP or GFP alone. Black arrow marks the cut site, white arrows mark the axon tip.

(F) Percentage of regenerating axons of hESC neurons. Error bars are s.e.m. P values indicate significance measured by ANOVA with Tukey's post-hoc analysis.

(G) Quantification of axon regeneration length. Error bars are s.e.m. Data were analysed by Student's T-test.

(H) Quantification of time to start of regeneration. Error bars are s.e.m. Data were analysed by Student's T-test.

Transgenic p110δ and p110α^{H1047R} support RGC survival and axon regeneration in the optic nerve

The data presented above confirm that p110δ behaves like the hyperactive p110α^{H1047R} mutant to generate elevated levels of axonal PIP3 and to facilitate CNS regeneration *in vitro*. In order to confirm whether p110δ and p110α^{H1047R} similarly support regeneration in the adult CNS *in vivo*, we used the optic nerve crush model to examine the effects of PI3K activation on regeneration of optic nerve axons after a crush injury. We used transgenic mice which conditionally express either p110δ or p110α^{H1047R} from the Rosa26 locus in the presence of Cre recombinase (Figure 6A), and delivered AAV2-Cre-GFP via intravitreal injection. Rosa26 is a safe harbour locus which allows expression of a transgene at moderate levels (Nyabi et al., 2009). Two weeks after viral injection, optic nerve crush was performed, and retinal ganglion

cell (RGC) survival and optic nerve regeneration were examined 28 days later (Figure 6B). We first tested AAV2-Cre-GFP activity using a Cre-reporter mouse line which expresses tdTomato from the Rosa26 locus (Figure S3A) and confirmed expression in p110δ and p110α^{H1047R} mice by examining GFP expression (from the viral vector) in the retina (Figure S3B). Activation of the PI3K/AKT/mTOR pathway was confirmed by phospho-S6 immunofluorescence. Expression of either p110δ or p110α^{H1047R} led to an increase in the number of cells labelling positive for phospho-S6, however p110α^{H1047R} expression led to a larger increase than p110δ expression (increasing to 80% for p110α^{H1047R}, and to 65% for p110δ, both from control levels of 45%) (Figure 6C and D). Despite this difference, p110δ and p110α^{H1047R} behaved similarly with respect to their effects on RGC survival. Optic nerve crush has dramatic effects on RGC viability so that by 28 days after the injury, only approximately 5% of neurons survive. The presence of transgenic p110δ or p110α^{H1047R} led to a doubling of the number of cells surviving after 28 days (from 5.5% to 11%), demonstrating a strong effect on cell survival (Figure 6E and F). We then measured axon regeneration in the optic nerve, and found that p110α^{H1047R} and p110δ again behaved similarly, both enabling a moderate increase in axon regeneration compared with control mice injected with AAV2-Cre.GFP (Figure 6G and H). The results confirm that p110δ and p110α^{H1047R} behave similarly in injured RGC neurons in the CNS *in vivo*, enhancing both RGC survival, and axon regeneration.

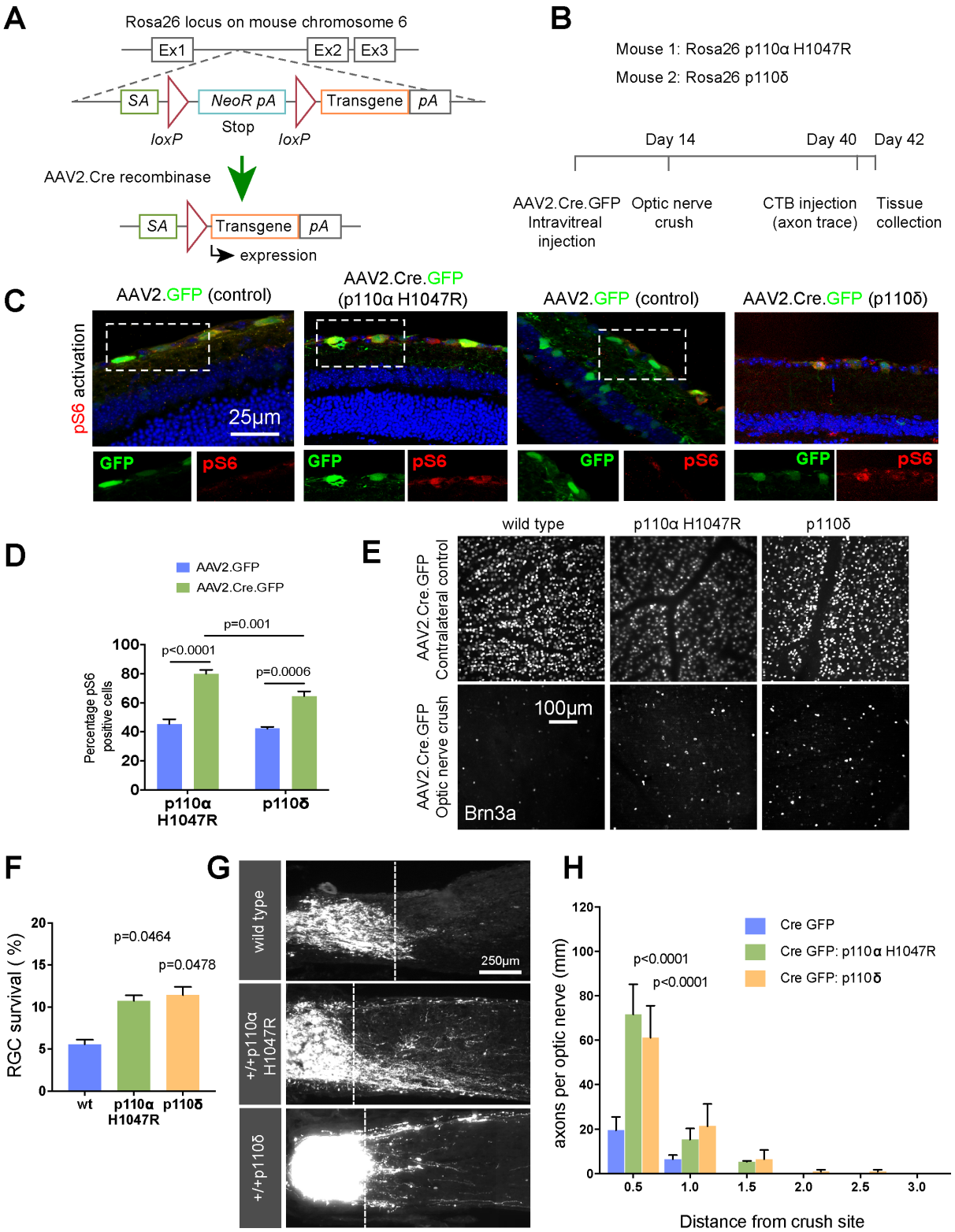
A
Rosa26 locus on mouse chromosome 6
Ex1
Ex2
Ex3
SA
NeoR pA
Transgene
pA
Stop
loxP
loxP
AAV2.Cre recombinase
SA
Transgene
pA
expression
B
Mouse 1: Rosa26 p110α H1047R
Mouse 2: Rosa26 p110δ
Day 14
Day 40
Day 42
AAV2.Cre.GFP Intravitreal injection
Optic nerve crush
CTB injection (axon trace)
Tissue collection
C
AAV2.GFP (control)
AAV2.Cre.GFP (p110α H1047R)
AAV2.GFP (control)
AAV2.Cre.GFP (p110δ)
pS6 activation
25μm
GFP
pS6
D
AAV2.GFP
AAV2.Cre.GFP
p=0.001
p<0.0001
p=0.0006
Percentage pS6 positive cells
p110α H1047R
p110δ
E
wild type
p110α H1047R
p110δ
AAV2.Cre.GFP Contralateral control
AAV2.Cre.GFP Optic nerve crush
100μm
Brn3a
F
RGC survival (%)
p=0.0464
p=0.0478
wt
p110α H1047R
p110δ
G
wild type
+/+p110α H1047R
+/+p110δ
250μm
H
Cre GFP
Cre GFP: p110α H1047R
Cre GFP: p110δ
p<0.0001
p<0.0001
axons per optic nerve (mm)
Distance from crush site

Figure 6.

Figure 6. p110δ and p110α^{H1047R} support RGC survival and axon regeneration in the optic nerve.

See also supplemental figure S3.

(A) Schematic representation of Rosa26 transgene expression via AAV.Cre recombinase.

(B) Time course of optic nerve regeneration experiments using Rosa26 p110α^{H1047R} and Rosa26 p110δ mice.

C) Retinal sections from AAV-injected mice, immunolabelled for phospho-S6.

(D) Percentage of phospho-S6 positive cells in the RGC layer 2 weeks after delivery of AAV-Cre-GFP or AAV-GFP. Error bars are s.e.m. P values indicate significance measured by ANOVA with Tukey's post-hoc analysis.

(E) Retinal whole mounts of AAV-injected mice immunolabelled for the RGC marker Brn3A to indicate cell survival.

(F) RGC survival 28 days after optic nerve crush. Error bars are s.e.m. P values indicate significance measured by ANOVA with Tukey's post-hoc analysis.

G) Representative images of CTB-labelled RGC axons 4 weeks after optic nerve crush in wild type (c57bl/6), Rosa26-p110α^{H1047R}, and Rosa26-p110δ transgenic mice injected with AAV2.Cre.GFP.

(H) Regenerating axons at different distances distal to lesion sites. Error bars are s.e.m. P values indicate significance as measured by ANOVA with Tukey's post-hoc analysis.

AAV2-p110δ facilitates axon regeneration in the optic nerve

The limited effects of transgenic p110 expression on axon regeneration in transgenic mice (described above) were surprising, given the robust effects of p110δ or p110α^{H1047R} expression on CNS axon regeneration *in vitro*. We reasoned that p110 enabled axon regeneration may be dose-dependent, and that the moderate expression generated from the Rosa26 locus (Nyabi et al., 2009) might explain these modest effects. In order to test whether these effects could be enhanced using a viral gene transfer approach, we produced an AAV2-p110δ construct for viral transduction of RGC neurons via intravitreal injection. We compared this with a similar AAV2-mediated shRNA approach to silence PTEN, the phosphatase responsible for opposing the actions of PI3K by dephosphorylating PIP3 to PIP2. Transgenic suppression of PTEN is

another means of stimulating regeneration in the CNS, however virus-mediated shRNA silencing has not proved to be as effective as transgenic deletion (Yungher et al., 2015). We therefore compared viral vector-based delivery of p110δ *versus* viral delivery of a PTEN targeting shRNA. We first confirmed that AAV2-shPTEN-GFP transduction resulted in silencing of PTEN in RGCs compared with neurons transduced with AAV2-scrambled-GFP control, as measured by quantitative immunofluorescence (Figure S4A and B). We confirmed transduction of RGCs by AAV2-p110δ by immunofluorescence, comparing p110δ fluorescence intensity with RGC neurons transduced with AAV2-GFP (Figure S4C and D). We next examined downstream signalling by labelling for phospho-S6 ribosomal protein. Transduction with AAV2-shPTEN-GFP led to an increase in the percentage of transduced cells labelling positive for phospho-S6 compared with AAV2-scrambled-GFP transduced neurons (from 27% for controls to 48% for PTEN silenced) (Figure 7A and B). Due to the lack of a fluorescent or epitope tag on AAV2-p110δ (due to potential effects on activity and packaging limits of the AAV), we measured the total number of TUJ1 labelled neurons that also labelled for phospho-S6. Transduction with AAV2-p110δ led to an increase in phospho-S6 positive neurons compared with AAV2-GFP transduced controls (1140 cells for p110δ transduced, compared with 650 cells for GFP transduced) (Figure 7A and C).

Having validated the two approaches, we next compared their effects on RGC survival and axon regeneration after optic nerve crush. Silencing of PTEN led to a robust increase in the survival of RGC neurons compared with controls at 28 days after crush (14.7% of PTEN silenced neurons survived compared with to 4.9% of control neurons), whilst transduction with p110δ led to a smaller effect on survival (11.3% of p110δ transduced neurons compared 6.3% of GFP control neurons) (Figure 7D and E), similar to the amount observed due to transgenic expression (Figure 6F). We next examined RGC axon regeneration in the optic nerve, and found that both AAV2 mediated silencing of PTEN and AAV2-delivery of p110δ enhanced

axon regeneration. Transduction with p110δ had the most robust effects on regeneration, with 180 axons counted at 0.5 mm into the optic nerve, compared with 25 axons in control-injected mice (Figure 7F). Injection of AAV2-shPTEN-GFP led to 97 axons at 0.5 mm, again compared with 25 axons for controls (this compares with 60 axons for p110δ, 70 for p110α^{H1047R} with transgenic expression). AAV2-p110δ also enabled axons to regenerate further into the optic nerve reaching a maximum distance of 3 mm, whilst silencing of PTEN only enabled axons to reach a maximum of 1.5 mm (transgenic expression of p110α^{H1047R} and p110δ also gave 1.5 mm regeneration). These data demonstrate that the PI3K pathway can be targeted to stimulate RGC survival and axon regeneration either by expressing p110δ or by silencing PTEN, and that expression of p110δ has the most robust effects on axon regeneration whilst silencing of PTEN has more sizeable effects on RGC survival/neuroprotection. Together these data show that enhancing PI3K activity in CNS neurons greatly enhances their ability to regenerate their axons, and indicate viral delivery of p110δ to CNS neurons as a novel approach to boost signalling through this regenerative pathway.

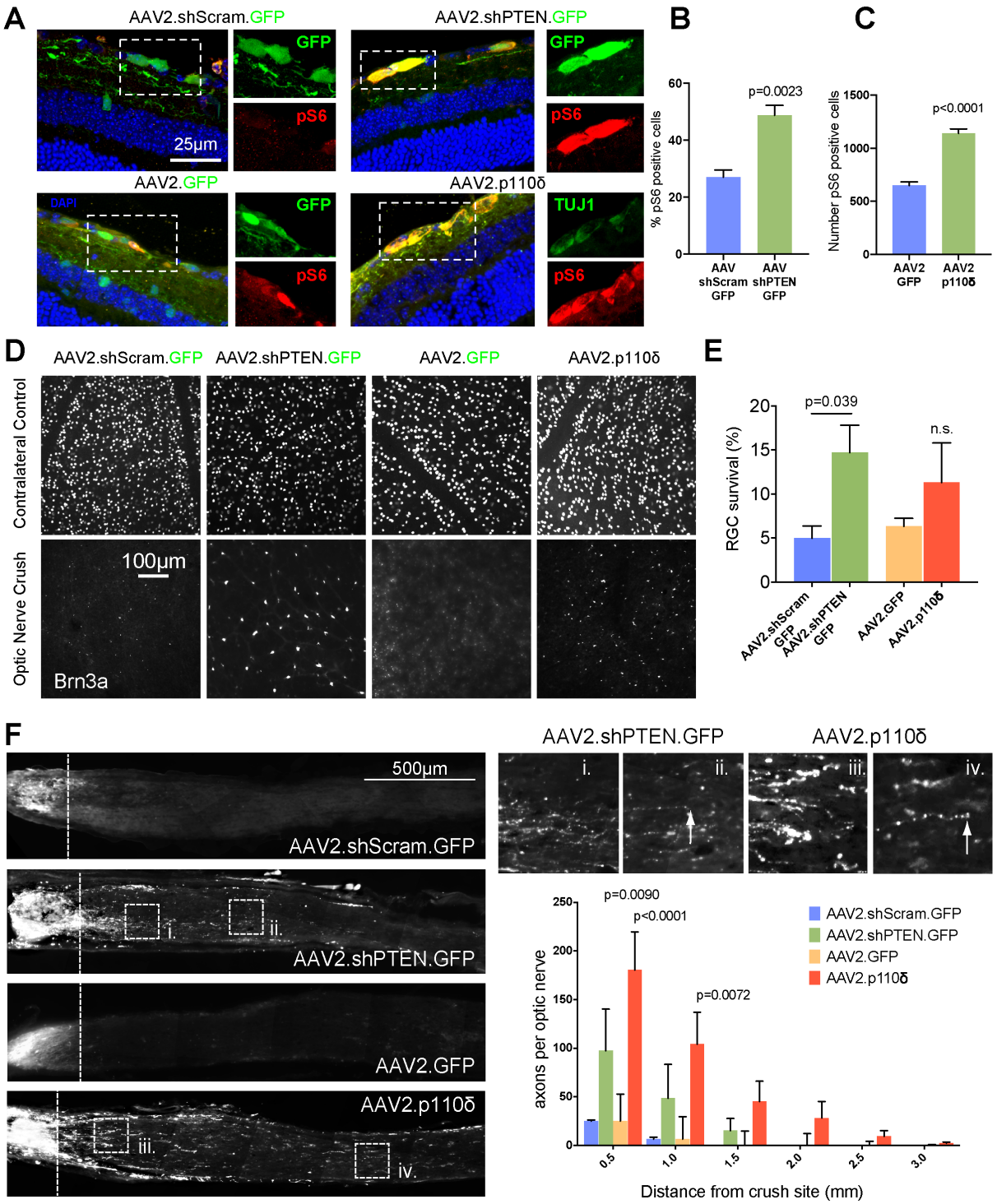
A
AAV2.shScram.GFP
AAV2.shPTEN.GFP
GFP
pS6
25µm
AAV2.GFP
AAV2.p110δ
DAPI
TUJ1
B
% pS6 positive cells
p=0.0023
AAV shScram GFP
AAV shPTEN GFP
C
Number pS6 positive cells
p<0.0001
AAV2 GFP
AAV2 p110δ
D
Contralateral Control
Optic Nerve Crush
100µm
Brn3a
E
RGC survival (%)
p=0.039
n.s.
AAV2.shScram GFP
AAV2.shPTEN GFP
AAV2.GFP
AAV2.p110δ
F
500µm
i.
ii.
iii.
iv.
axons per optic nerve
p=0.0090
p<0.0001
p=0.0072
Distance from crush site (mm)

Figure 7.

Figure 7. AAV2-p110δ facilitates axon regeneration in the optic nerve.

See also supplemental figure S4.

(A) Retinal sections from mice injected with AAV2 viruses as indicated, immunolabeled for phospho-S6.

(B) Percentage of phospho S6 positive cells in the retinal ganglion layer of mice injected with AAV2.shScramble.GFP or AAV2.shPTEN.GFP. Error bars are s.e.m. P values indicate significance measured by Students T-test.

(C) Number of pS6-postive RGCs of mice injected with AAV2.GFP or AAV2.p110δ. Error bars are s.e.m. P values indicate significance measured by Students T-test.

(D) Representative images of retinal whole mounts from AAV-injected mice stained for the RGC marker Brn3A to indicate RGC survival.

(E) RGC survival 28 days after optic nerve crush. Error bars are s.e.m. P values indicate significance as measured by ANOVA with Tukey's post-hoc analysis.

(H) CTB-labelled RGC axons 4 weeks after optic nerve crush. Boxes i. to iv. show regenerating axons. White arrows mark the end of axons. Graph shows quantification of regenerating axons at different distances distal to the lesion sites. Error bars are s.e.m. P values indicate significance measured by ANOVA with Tukey's post-hoc analysis.

Discussion

Our study demonstrates that robust axon growth and regeneration can be driven by high levels of axonal PIP3. In developing CNS and adult PNS neurons PIP3 levels are high, and inhibiting PI3K reduces axon growth and regeneration. Conversely, mature CNS neurons have low levels of PIP3, and introduction of either p110δ or p110α^{H1047R} raises PIP3 levels in both the cell body and axon, leading to increased regenerative ability.

Developing CNS neurons exhibit intense PIP3 levels at the growth cone during the period of rapid axon growth, but this is downregulated at a time when axons lose their capacity for regeneration. Overexpression of p110δ or p110α^{H1047R} in mature CNS neurons partially restored PIP3 levels, particularly in axon tips, and also restored regenerative ability *in vitro*,

both in rat cortical neurons and in human stem cell neurons. p110δ and p110α^{H1047R} also behave similarly in the CNS *in vivo*, with transgenic expression leading to enhanced neuroprotection in the retina, and regeneration in the optic nerve after a crush injury. Importantly, viral transduction of p110δ into adult RGC neurons leads to axons regenerating for a greater distance after injury, demonstrating a novel approach to boost CNS regeneration through the PI3K pathway by gene transfer. Previous work has indicated that the hyperactive H1047R mutation of p110α can behave like p110δ to sustain AKT signalling in fibroblasts, by functioning independently of co-activation by Ras (Kang et al., 2006). Crucially, expression of native p110α had no effect on PIP3 generation, it was only p110δ or p110α^{H1047R} that enhanced axonal PIP3 (Figure 3). This suggests that receptor activation of PI3K is at a low level in mature CNS neurons, and that p110δ can potentiate PI3K signalling in low trophic conditions that are insufficient to activate native p110α. Our findings suggest that p110δ has a lower threshold of activation and that additional signals normally required to fully activate p110α (such as Ras) may not be available in the axon. This has important implications for understanding the nature of p110δ beyond the nervous system, and may help to explain how T-cells utilise p110δ for development, differentiation and function (Okkenhaug, 2013). The phospholipid fixation protocol that we describe here has been instrumental in characterising both the nature and localisation of PI3K activity in neurons, and will no doubt prove useful for research into PI3K function in other cell types.

The PI3K signalling pathway is a well-known regulator of axon regeneration, based on seminal studies which demonstrated that deletion of PTEN leads to robust regeneration in the CNS through downstream signalling via mTOR (Park et al., 2008). Aside from mTOR, the mechanism through which PTEN deletion stimulates regeneration is not completely understood. One difficulty in understanding its mechanism is that in addition to functioning as a lipid phosphatase (PTEN opposes PI3K by converting PIP3 back to PIP2) it also has protein

phosphatase activity (Kreis et al., 2014). It is now also apparent that PTEN not only dephosphorylates PI(3,4,5)P_3, but also functions as a PI(3,4)P_2 phosphatase, a role linked with cancer invasion (Malek et al., 2017). Our findings argue in favour of PTEN functioning through the regulation of PIP3, and confirm the importance of this molecule in the regulation of axon regeneration.

Most PI3K signalling events rely on more than one isoform (Hawkins and Stephens, 2015), and whilst the p110δ isoform contributes to sciatic nerve regeneration (Eickholt et al., 2007), the contribution of the other isoforms remained unknown. Our findings demonstrate that both p110α and δ are required for efficient axon regeneration, and that p110α functions in both the axon and cell body, whilst p110δ is specifically required in the axon (Figure 1). Inhibition of p110α opposed both axon growth and regeneration, whilst the action of p110δ was specific to regeneration, with the p110δ inhibitor blocking regeneration but not growth of uncut axons. Taken together, these results suggest that p110α mediates the somatic and axonal signalling that is necessary to support adult DRG axon growth (itself a regenerative phenomenon), whilst p110δ is further required within the axon to facilitate the redevelopment of a growth cone after injury. In CNS neurons, overexpression of either p110δ or p110α^{H1047R} was sufficient to enable efficient regeneration both *in vitro* and *in vivo,* and AAV mediated p110δ expression in RGCs promoted robust optic nerve regeneration.

Our findings demonstrate the importance of PIP3 in the axon as well the cell body for optimal regeneration. Studies targeting the PTEN/PI3K pathway for CNS axon regeneration examined downstream activation by measuring ribosomal S6 phosphorylation in the cell body (Duan et al., 2015; Liu et al., 2017; Park et al., 2008; Smith et al., 2009), so it is difficult to determine whether these interventions also lead to axonal signalling. The observed increase in axonal PIP3 caused by expression of either p110δ or hyperactive p110α^{H1047R} may be a result of increased axon transport of PI3K-coupled receptors, such has been demonstrated for TrkB

in response to BDNF. This feed-forward mechanism functions through PI3K to ensure an axonal presence of receptors during developmental axon growth (Cheng et al., 2011). Although deletion of PTEN enhances regeneration via mTOR signalling in the cell body, mTOR has recently been found to be present at the growth cone of developing axons in the mouse cerebral cortex, suggesting the PI3K-AKT-mTOR pathway may also function locally within the axon (Poulopoulos et al., 2019). It is important however to note that signalling through mTOR only represents a subset of the signalling molecules regulated downstream of PIP3 or PIP2. PIP3 and PIP2 exert their effects via a wide variety of proteins with PH domains that may also contribute to regenerative effects, including the regulatory molecules of small GTPases that regulate the cytoskeleton, such Rac1 and Cdc42 (Sosa et al., 2006; Welch et al., 2002; Yoshizawa et al., 2005), or that regulate axon transport such as ARF6 and Rab11 (Gillingham and Munro, 2007; Nieuwenhuis and Eva, 2018). Enhancing PI3K signalling may therefore promote the axonal transport and trafficking of a range of axon growth-promoting molecules that are normally excluded (Eva et al., 2017; Hollis et al., 2009a; Hollis et al., 2009b). The importance of targeting the axon as well as the cell body is often overlooked, however there is increased axonal transport as part of the PNS injury response and in the CNS, increased transport enables regeneration (Petrova and Eva, 2018).

The search for translatable methods for promoting regeneration in the damaged CNS continues. A successful strategy will likely involve multiple interventions. Could manipulation of PI3K be translationally useful? PTEN deletion or p110α^{H1047R} expression can be oncogenic in dividing cells. However, expression under a neuron-specific promoter targets expression to a non-dividing cell type, and it is unlikely that expression of p110δ in CNS neurons would lead to cell transformation, particularly given its usual expression in PNS neurons. Our study puts forward AAV-mediated delivery of p110δ as a novel means of stimulating regeneration through the PI3K pathway in a potentially translatable fashion. We propose that p110δ should

also be considered as an additional intervention with other regenerative strategies that target the PI3K pathway, either through genetic treatment such as osteopotin and IGF-1, (Duan et al., 2015; Liu et al., 2017), expression of activated integrins (Cheah et al., 2016) or pharmacological interventions such as insulin (Agostinone et al., 2018).

Acknowledgements

We acknowledge the Babraham Institute Gene Targeting facility for the generation of the Rosa26 p110 mouse strains, and would like to thank Dr. Len Stephens and Dr. Phill Hawkins (Babraham) for the gift of the GFP-AKT-PH mouse strain, and for their advice and support. The work was supported by grants from MRC-Sackler, International Spinal Research Trust (NRB110), Wellcome Trust, ERA-NET NEURON grant AxonRepair (013-16-002), Medical Research Council MRC (MR/R004544/1, MR/R004463/1), Christopher and Dana Reeve Foundation, Cambridge Eye Trust, Fight for Sight, NERC and a core support grant from the Wellcome Trust and MRC to the Wellcome Trust – Medical Research Council Cambridge Stem Cell Institute. B.J.E. funding was provided by the DFG (SFB 958, TP16; SFB TRR 186, TP10). S.v.E was funded by EMBO ALTF 1436-2015, and S.v.E & C.ff-C by MS Society UK. K.O. laboratory funding was provided by the BBSRC and the Wellcome Trust.

Author contributions

A.C.B, R.S.E, B.N., C.S.P, J.F, P.D.S, S.v.E and R.E. performed and analysed experiments. A.R.M generated PI3K transgenic mice. B.H., A.O. and L.A.H. generated AAV.p110delta. R.C. J.C. and S.S.D. analysed RGC survival. K.O. designed and supervised transgenic generation of mice. B.J.E designed and supervised PIP3 detection experiments. R.E., J.W.F, K.R.M, A.C.B, C.ff-C, S.v.E, B.J.E and K.O. conceived designed and supervised experiments

and obtained funding. R.E., B.N., A.C.B. and R.S.E prepared movies and figures. R.E. wrote the manuscript.

Declaration of Interests

KO received consultancy payments and/or research funding from Karus Therapeutics, Gilead Sciences and GlaxoSmithKline.

Materials and Methods

Mouse Strains

C57BL6/J mice were used during this study, as well as four transgenic mouse strains: GFP-AKT-PH, Rosa26 p110α^{H1047R}, Rosa26 p110δ and B6;129S6-Gt(ROSA)26Sortm14(CAG-tdTomato)Hze/J (https://www.jax.org/strain/007908). The generation of the PIP3 reporter mouse GFP-AKT-PH has been previously described (Nishio et al., 2007) and was a gift from Dr Len Stephens (Babraham Institute, UK). Male and female mice were used dependent on litters available with equal distributions across experiments. Rosa26 p110α^{H1047R}, Rosa26 p110δ were generated according to a previously described protocol (Nyabi et al., 2009). Briefly, cDNA sequences for human p110α or p110δ were cloned into the pENTR D-TOPO vector (ThermoFisher) to allow cloning into Gateway-compatible vectors. The H1047R point mutation was introduced by site-directed mutagenesis into PIK3CA using the Quickchange II XL kit (Stratagene #200521) and the primers Quickchange H1047R forward 5'-catgaaacaaatgaatgatgcacgccatggtggctggacaac-3', Quickchange H1047R reverse 5'-gttgtccagccaccatggcgtgcatcattcatttgtttcatg. Presence of the mutation was confirmed by sequencing prior to cloning into the destination vector. PIK3CD (p110δ) was a gift from Roger Williams (MRC Laboratory for Molecular Biology, UK). PIK3CA (p110α) was a gift from Bert Vogelstein (Addgene plasmid #16643 ; http://n2t.net/addgene:16643; RRID:Addgene_16643) (Samuels et al., 2004). The Gateway®-compatible pROSA26 destination vector (pROSA26-DV1) was a gift from Jody Haigh (University of Manitoba, Canada) (Nyabi et al., 2009). Targeting constructs harbouring sequences for p110α^{H1047R} or p110δ were used to electroporate Bruce4 C57BL/6 ES cells. Selection of targeted clones was undertaken with G418, making use of the neomycin resistance selection cassette. Positively targeted clones were identified by Southern blotting. Positively targeted clones were microinjected into C57BL/6J-Tyrc-2J blastocysts by Babraham Institute Gene Targeting

Facility (Babraham Institute, UK). These blastocysts were transferred to the oviducts of time-mated pseudopregnant foster mothers. The progeny were assessed for their degree of chimerism by coat colour and chimeric males mated to white C57BL/6J-Tyrc-2J females. Black progeny were tested for their correct incorporation of the Human PI3K genes at the Rosa26 locus by PCR using the following primers:

Rosa26 Hs p110	ROSA26 F1 AMQ	GGCTCAGTTGGGCTGTTTTG	WT allele = 359 bp KI allele = 603 bp
	ROSA26 R2 AMQ	TCTGTGGGAAGTCTTGTCCC	
	ROSA26 loxP AMQ	GTGGATGTGGAATGTGTGCG	
Hs p110α	Hs PIK3CA #5 intra fwd	TTGATCTTCGAATGTTACCT	KI allele = 813 bp
	S2rev	CTTGATATCGAATTCCGCCCC	
Hs p110δ	Hs PIK3CD #5 intra fwd	GTACTCCGTTCAGACACCAT	KI allele = 742 bp
	S2rev	CTTGATATCGAATTCCGCCCC	

Adult rat and mouse DRG culture

Dissociated DRG neuronal cultures were obtained from adult male Sprague Dawley rats and from the transgenic AKT-PH-GFP adult mouse. The method was the same for both species. DRGs were incubated with 0.1% collagenase in Dulbecco's modified Eagle's medium (DMEM) for 90 min at 37°C followed by 10 min in trypsin at 37°C. DRGs were dissociated by trituration in a blunted glass pipette. Dissociated cells were then centrifuged through a layer of 15% bovine serum albumin (BSA), washed in DMEM, and cultured on 1 µg/ml laminin on poly-D-lysine-coated glass-bottom dishes (Greiner) in DMEM supplemented with 10% fetal calf serum, 1% penicillin-streptomycin and 50 ng/ml nerve growth factor (NGF). For compartmentalised experiments, DRG neurons were plated in Xona microfluidic devices (Xona SND150) cultured on glass coverslips. Dissociated adult DRG neurons were floated inside the channels of the device, which was adhered to the cover glass, and cultured with the usual medium. For PI3K inhibitor experiments, media was exchanged for serum free media

overnight in advance of the axotomy experiment. Separation of media was achieved by maintaining a pressure gradient between the axonal and somatic side of the device. When inhibitors were added to the soma side, a greater volume of media was added to the axonal side. For inhibition of only the axons, a greater volume was maintained on the soma side.

Embryonic rat cortical neuron culture

Primary rat cortical neuron culture has been described previously (Eva et al., 2017). Cultures were prepared from embryonic day 18 (E18) Sprague Dawley rats. Neurons were dissociated with papain for 8 min at 37°C, washed with HBSS and cultured in MACS Neuromedium supplemented with MACS Neurobrew (Miltenyi). Cells were plated on glass-bottom dishes (Greiner) coated with poly-D-lysine. Culture dishes were incubated in humidified chambers to prevent evaporation of culture medium, allowing long-term culture [up to 28 days *in vitro* (DIV)]. Cells were transfected at 10 DIV, and experiments (imaging or axotomy) were performed between 14 and 17 DIV. Cortical neurons were transfected by oscillating nano-magnetic transfection (magnefect nano system, nanoTherics, Stoke-On-Trent, UK) as previously described (Franssen et al., 2015).

hESC dopaminergic neuron culture

RC17 hESC cell culture has been have been previously described in detail before (De Sousa et al., 2016; Koseki et al., 2017). Cells (RRID:CVCL_L206) were sourced from Roslin Cells, Scottish Centre for Regenerative Medicine, Edinburgh, United Kingdom. The cell line is free from mycoplasma contamination as determined by RT-qPCR. On d0 hESC were detached and transferred to form embryoid bodies from d0 to d4 in neural induction medium (Neurobasal:DMEM/F12 (1:1), 0.2% P/S, L-glutamine, N2, B27, recombinant Sonic Hedgehog Shh (C24II), recombinant noggin (Ng), SB431542 (SB) and CHIR99021 (CH). Rock inhibitor (RI,) was present in the medium from d0 to d2. At d4, embryoid bodies were

plated in poly-L-ornithine Laminin and Fibronectin (PLF) coated plates and cultured in neural proliferation medium (Neurobasal:DMEM/F12 (1:1), 0.5xN2, 0.5xB27, supplemented with Shh, Ng, SB and CH from d4-d7, and with Shh, Ng and CH from d7-d9). At d11, cells were dissociated with Accutase and 50*104 cells per well single cell suspensions were plated in PLF-coated 8-well chamber slides. Cells were cultured in neuronal differentiation medium (NB with 0.2% P/S, l-glutamine, B27, Ascorbic Acid, recombinant human Brain-derived Neurotrophic Factor, Glial-cell line derived Neurotrophic Factor (GDNF) which was further supplemented with Dibutyryladenosine 3', 5'-cyclic monophosphate sodium salt (db-CAMP; 50 mM) and DAPT from d14 onwards. Medium was replaced twice weekly up to day 50, after which medium was replaced weekly.

N1E Cell Culture

N1E-115 cells (ATCC) were plated at a density of 5.000 cells / cm^2 in DMEM-high glucose with GlutaMAX (Gibco) + 10% FBS with antibiotics and incubated for 6-7 h at 5% CO_2 and 37°C.

DNA Constructs

Constructs for expressing the various isoforms of p110 were generated from pHRsinUbEm, a bicistronic vector, expressing EGFP under the control of the SFFV promoter and emerald fluorescent protein under the control of the Ubiquitin promoter. p110δ (PIK3CD) was a gift from Roger Williams (MRC Laboratory for Molecular Biology, UK). PIK3CD was cloned from pcDNA3.1 in place of EGFP, first removing EGFP by restriction digest with BamH1 and Not1. p110α (PIK3CA) and p110α H1047R were cloned into the same site from pBabe puro vectors. pBabe puro HA PIK3CA and were gifts from Jean Zhao (Addgene plasmid #12522 and #12524; http://n2t.net/addgene:12522 ; RRID:Addgene_12522,

http://n2t.net/addgene:12524 ; RRID:Addgene_12524) (Zhao et al., 2005). AAV.CAG.p110δ was generated by cloning the human PIK3CD sequence into an AAV-sCAG vector backbone by Gibson assembly (Gibson et al., 2009).

Antibodies

PI(3,4,5)P: anti-PtdIns(3,4,5)P_3 monoclonal antibody (Z-P345b, 1:200, Echelon Biosciences), GFP (rabbit, 1:500 Abcam ab290), phospho-S6 ribosomal protein (Ser235/236) (91B2) (rabbit, 1:200, Cell Signaling 4857S), TUJ1(βIII Tubulin) (mouse, 1:400, Promega G7121), PTEN (D4.3) XP (rabbit, 1:100, Cell Signalling 9188S), p110δ (rabbit, 1:500, Abcam ab1678), Brn3a (C-20) (goat, 1:200, Santa Cruz sc-31984). Anti-goat Alexa Fluor-647 (1:1000, A21447, Life technologies). Anti-rabbit IgG conjugated Alexa Fluor 568 (A10042, 1:1000, ThermoFischer scientific). Anti-mouse IgG conjugated Alexa Fluor 568 (A11004, 1:1000, ThermoFischer scientific). Anti-rabbit IgG conjugated Alexa Fluor 488 (A-21206, 1:1000, ThermoFischer scientific). Anti-mouse IgG conjugated Alexa Fluor 488 (A-21202, 1:1000, ThermoFischer scientific).

Small molecule inhibitors

The following small molecule inhibitors were used to inhibit the various isoforms of PI3 kinase p110. The indicated concentrations were chosen as relatively high doses based on their known IC50, and from previously reported cell culture experiments: Pan-p110 (p110α/β/δ): LY294002 20 μM (IC50 (in cell free assays) 0.5 μM/0.97 μM/0.57 μM, respectively). p110α: A66 5 μM (IC50 32nM). p110α/δ: XL-147 5 μM (IC50 39 nM/ 36nM). p110β: TGX221 500 nM (IC50 5 nM). p110δ: IC-87114 10μM (IC50 0.5 μM). p110δ: Idelalisib 500 nM (IC50 2.5 nM).

Virus production and injection

Three viruses were sourced commercially: AAV2.CMV.Cre.GFP (Vector Biolabs, Catalog #7016), AAV2.CMV.GFP (Vigene Biosciences, Catalog #CV10004) and AAV2.U6.shRNA(scramble).CMV.GFP (SignaGen Labs, Catalog #SL100815). AAV2.U6.shPTEN.CMV.GFP, was a gift from Zhigang He, (Boston Children's Hospital) and AAV2.CAG.p110delta was produced by Vigene Biosciences.

Mice received 2 µl intravitreal injections of AAV. All viruses were injected into the left eye only at a titre of 1 x 10^{13} GC/ml, using sterile PBS to dilute if necessary. In validation experiments, the mice received a 2 µl intravitreal injection into the left eye of either AAV2.Cre.GFP, AAV2.shPTEN.GFP or AAV2.p110δ, and also received intravitreal injection of the appropriate control into the right eye: AAV2.GFP, AAV2.shScram.GFP or AAV2.GFP respectively. In addition, the Td-Tomato-Crereporter mice received a 2 µl intravitreal injection of AAV2.Cre.GFP into the left eye. These mice were perfused 2 weeks later and whole eyes were collected.

Optic nerve injury

Animal work was carried out in accordance with the UK Home Office regulations for the care and use of laboratory animals, the UK Animals (Scientific Procedures) Act (1986), and the Association for Research in Vision and Ophthalmology's Statement for the Use of Animals in Ophthalmic and Visual Research. Surgical procedures were performed under anesthesia using intraperitoneal injection of ketamine (100 mg/kg) and Xylazine (10 mg/kg).

Two weeks after AAV2 injection, optic nerve injuries were carried out as previously described (Smith et al., 2009). The optic nerve behind the left eye was exposed intraorbitally, and crushed with fine forceps for 10 sec, approximately 0.5 mm behind the optic disc. 26 days after the injury, mice received a 2 µl intravitreal injection of cholera toxin subunit β (CTB) with an

Alexa Fluor 555 conjugate diluted with sterile PBS to a concentration of 1mg/ml. At 28 days post crush, animals were perfused with 4% paraformaldehyde (PFA) and the eyes and optic nerves were collected for analysis.

Immunohistochemistry

Retinas were fixed in 4% PFA for 2 h and transferred to PBS for immunohistochemistry. Whole-mounts were washed four times with 0.5% PBS-TritonX100. In between the second and third wash, a permeation step was performed to improve antibody penetration by freezing the retinas in 0.5% PBS-TritonX100 for 10 min at -70°C, and washing was continued after thawing. Optic nerves were collected and fixed overnight at 4°C in 4% PFA, followed by 30% sucrose overnight at 4°C. Sections were blocked with 2% BSA, 10% donkey serum in 2% PBS-TritonX100. Primary antibodies were incubated at 4°C overnight, secondary antibodies for 2 h at room temperature.

Standard immunocytochemistry

Cortical neurons were fixed with 3% paraformaldehyde (PFA) in PBS for 15 min and permeabilized with 0.1% Triton X-100 in PBS for 5 min. Cells were blocked with 3% bovine serum albumin (BSA) in PBS for 1 h. After blocking, the cells were incubated with primary antibodies diluted in 3% BSA in PBS at 4°C overnight. Secondary antibodies that were diluted in 3% BSA in PBS for 1 h at room temperature. Cells were mounted using Fluorsave (Calbiochem, 345789).

Phospholipid fixation and immunocytochemistry

We adapted a fixation technique previously used to detect PI(4,)P_2 and PI(4,5)P_2 (Hammond et al., 2009). Cortical neuron cultures were fixed using a pre-warmed (37°C) mixture of 3%

formaldehyde and 0.2% glutaraldehyde (GA; G011/3, TAAB Laboratories) in PBS for 15 min at room temperature. After fixation, cells washed in 50 mM ammonium chloride (NH_4Cl) in PBS, and moved to the cold room (4°C) for subsequent immunocytochemistry (to reduce diffusion of the non-fixable membrane lipids). Cells were incubated with pre-chilled blocking and permeabilisation solution (0.2% saponin, 50 mM NH_4Cl and 3% BSA in PBS) for 30 min at 4°C. The cells were then incubated with purified anti-PtdIns(3,4,5)P3 monoclonal antibody (Z-P345b, 1:200, Echelon Biosciences) in blocking solution for three h at 4°C before washing three times in 50 mM NH_4Cl in PBS for a total of 30 min at 4°C. Secondary antibody was applied in the same blocking buffer and incubated for 2 h at 4°C. After another 30 min wash, cells were post-fixed in 3% formaldehyde in PBS for 5 min at 4°C before being moved to room temperature and fixed for a further 10 min. After post-fixation, the cells were washed at room temperature and mounted using Fluorsave reagent.

Insulin Stimulation of N1E cells

Cells were then starved in DMEM without serum overnight in the presence of either 500 nM GDC-0941 (Selleckchem) or an equal volume of cell-culture grade DMSO (Applichem). Cells were stimulated with 20 µg/ml insulin (Sigma) in DMEM or control treated with equal amounts of DMEM for 1 min prior to fixation in PIP3-Immobilization fixative and stained with for PIP3 (anti-PIP3, Echelon) and F-actin (Phalloidin, Thermo Fisher Scientific).

Confocal and widefield microscopy

Laser-scanning confocal microscopy was performed using a Leica DMI4000B microscope, with laser scanning and detection achieved by a Leica TCS SPE confocal system controlled with Leica LAS AF software. Fluorescence and wide-field microscopy were performed using a Leica DMI6000B with a Leica DFC350 FX CCD camera and a Leica AF7000 with a Hamamatsu EM CCD C9100 camera and Leica LAS AF software. Leica AF7000 was also

used for imaging of axon and growth cone regeneration after axotomy. N1E cell imaging was performed on a Leica SP5 confocal system with a 40x Objective.

TIRF Microscopy

Total internal reflection fluorescence (TIRF) microscopy was carried out on a Leica DMI6000B microscope adapted with a dedicated TIRF module from Rapp OptoElectronic. GFP was excited with a 488 nm laser and images were acquired using a Leica Plan Apo 100x / NA1.47 Oil TIRF objective and Hamamatsu EM CCD C9100 camera controlled by Leica LAS AF and Rapp OptoElectronic software.

Laser axotomy of DRG neurons

Laser axotomy DRG neurons was performed as described previously (Eva et al., 2017). Adult DRG neurons were axotomised directly before a growth cone, to determine the proportion of axons that regenerate a growth cone rapidly after injury. Adult DRG cultures were serum starved overnight, and PI3K inhibitors were added at the start of the experiment and maintained throughout. Axons were severed using a 355 nm DPSL laser (Rapp OptoElectronic, Hamburg, Germany) connected to a Leica AF7000 microscope, and images were acquired every 15 min for a period of 2 h. Successful regeneration was determined as the development and extension of a new growth cone. Time taken to develop a new growth cone was also recorded.

Laser axotomy of cortical neurons

Laser axotomy of cortical neurons was performed as described previously (Eva et al., 2017; Koseki et al., 2017) Axons were severed in vitro using a 355 nm DPSL laser (Rapp OptoElectronic, Hamburg, Germany) connected to a Leica DMI6000B microscope. Cortical neurons were axotomised at DIV 14–17 at distances of 800–2000 μm distal to the cell body on a section of axon free from branches. In this way, axons were cut at a substantial distance from

the cell body, but not close to the end of the axon. For these experiments, neurons were transfected at DIV 10. Neurons were visualised by virtue of the GFP fluorescent signal. Only highly polarised neurons (with many dendrites and a single axon) were chosen. A single axon cut was made per neuron. Images after axotomy were acquired every 30 min for 14 h. Regeneration was classed as the development of a new growth cone followed by axon extension for a minimum of 50 µm.

Laser axotomy of hESC-derived neurons

Laser axotomy of hESC-derived neurons was performed as described previously (Koseki et al., 2017). Axons were severed in vitro using a 365 nm laser (Micropoint, Andor) connected to a Andor spinning disk confocal microscope. Neurons were axotomised at d45-65 at distances of >500µm distal to the cell body on a section of axon free from branches. For these experiments, neurons were transfected 2-3 days prior to axotomy. Neurons were visualised by virtue of the GFP fluorescent signal. Only highly polarised neurons (with many dendrites and a single axon) were chosen. A single axon cut was made per neuron. Images after axotomy were acquired every 20 min for 16 h. Regeneration was classed as the development of a new growth cone followed by axon extension for a minimum of 50 µm.

Quantification of PIP3 in cortical neurons

For developmental analysis, E18 cortical neurons were fixed at DIV 3, 8, or 16 and PIP3 was detected using phospholipid fixation a PIP3 antibody as described above. All cultures were fixed and labelled using identical conditions. Images were acquired by confocal laser-scanning microscopy using a Leica TCS SPE confocal microscope. Identical settings were used for the acquisition of each image using Leica LAS AF software. Z-stacks were acquired for each image, spanning the entire depth of either the cell body or the growth cone. PIP3 fluorescence intensity was measured at cell bodies axonal growth cones using Leica LAS AF software. All

immunofluorescence intensities were calculated by measuring the intensity of the region of interest (ROI), and then subtracting the intensity of a control region adjacent to the ROI.

Quantification of PIP3 in N1E cells

Imaging was performed on a Leica SP5 confocal system with a 40x Objective with identical laser intensities and PMT-gains across experiments. Stacks covered the complete height of all cells with a z-Interval of 1 µm. Areas with comparable cell densities were selected in the F-actin channel. Mean PIP3 intensity in N1E cells was quantified in Fiji (ImageJ 1.51n) on max-projections. Intensities were compared in 15 images per treatment from 3 independent cultures.

Analysis of neuronal morphology

Images for neuronal morphology of 14 DIV neurons were captured on a Leica DMI6000B, with a 40X-oil objective using Leica LAS AF. Semi-automated and standardized analysis of neuronal morphology was performed using MATLAB platform version 2017 and the program SynD (Schmitz et al., 2011). SynD detects the soma by thresholding and component analysis and afterwards detects the neurites by applying steerable filters at the immunofluorescence images. Neurites that were not completely traced were manually traced and crossing neurites from of different neurons were manually removed. The output of SynD was used for data analysis of dendritic length, fluorescent intensities, sholl analysis, and soma size.

Neurite outgrowth assay

Cultured cortical neurons were transfected at 2 DIV and fixed and immunolabelled at 4 DIV to enhance the eGFP fluorescence intensity. Images for neuronal morphology were acquired using a Leica DMI6000B microscope, with a 40X-oil objective using Leica LAS AF. Neurite lengths were measured using the ImageJ plugin ‘simple neurite tracer’(Longair et al., 2011).

Optic nerve regenerating axon counts

To measure regenerating RGC axons after optic nerve crush, longitudinal sections of optic nerves were serially collected. Regenerating RGC axons were quantified as described previously (Smith et al., 2009), by counting the number of CTB labelled axons at the indicated distances beyond the crush site from 4 sections per optic nerve. Axonal sections were imaged using a Zeiss AxioScan Z1 at x40 magnification.

RGC survival counts

Following cardiac perfusion, the retinas were extracted from the collected eyes and flattened into whole-mounts, facilitated by four cuts to enable the tissue to lie flat. The retinas were fixed in 4% PFA for 2 h and transferred to PBS for immunohistochemistry as described above. For the retinal whole-mounts, 2 images were taken from each of the four retinal quadrants at x20 magnification, sampling both the more central and the more peripheral region of each quadrant. Images were then analysed in Image J Fiji using Image-Based Tool for Counting Nuclei (ITCN) Plugin (University of California, Santa Barbara, CA, USA) to count Brn3A-labelled cells. The number of RGCs in the left injured eye was expressed as a percentage survival value compared to the mean number of RGCs of the contralateral control eyes.

RGC fluorescence analysis

To confirm successful viral transduction in vivo, eye cup images were produced from the retinal sections injected with each virus, stained either GFP or PI3KDelta and counterstained with DAPI, using a Zeiss AxioScan Z1 at x20 magnification. From the same sections, the RGC layer was also imaged by confocal microscopy (as described above). Retinal sections immunolabelled for pS6 were examined by fluorescence microscopy. 100 GFP-positive RGCs (identified using GFP signal from viruses) were counted and identified as positive or negative

for pS6 across 4 mice of each group. For AAV2.p110δ transduced RGCs, the total number of pS6 positive cells was counted across the eye from 12 retinal sections taken throughout the eye per mouse and compared to total number of pS6 positive cells from the control group using TUJ1as a marker of RGC neurons. To quantify PTEN knockdown, retinal sections injected with AAV2.U6.shPTEN.CMV.GFP or AAV2.U6scram.CMV.GFP, were immunolabelled for PTEN magnification using confocal microscopy, and fluorescence intensity of PTEN was quantified in transduced RGCs identified by GFP fluorescent signal. Fluorescence intensity was measured using ImageJ FIJI. The AAV2.U6.shPTEN.CMV.GFP shRNA construct has been previously described and validated (Luikart et al., 2011; Xin et al., 2005; Zukor et al., 2013). To quantify p110δ transduction, retinal sections injected with either AAV2.CAG.p110δ or AAV2.CMV.GFP, immunolabelled for p110δ, and images were acquired by confocal microscopy and fluorescence intensity was measured in TUJ1 labelled RGCs using ImageJ FIJI.

Quantitative and Statistical Analysis

Statistical analysis was performed throughout using Graphpad Prism. Fisher's exact test was calculated using Graphpad online (https://www.graphpad.com/quickcalcs/contingency1.cfm). Data were analysed by ANOVA with post hoc analysis, Student's t-test and Fisher's exact test. Sample sizes were based on previously published data using similar techniques. Statistical analysis was performed using ANOVA followed by Tukey's multiple comparison test or Student’s T-test, as indicated in the figure legends. Percentage of regenerating axons was compared by Fisher's exact test.

References

Agostinone, J., Alarcon-Martinez, L., Gamlin, C., Yu, W.Q., Wong, R.O.L., and Di Polo, A. (2018). Insulin signalling promotes dendrite and synapse regeneration and restores circuit function after axonal injury. Brain 141, 1963-1980.

Al-Ali, H., Ding, Y., Slepak, T., Wu, W., Sun, Y., Martinez, Y., Xu, X.M., Lemmon, V.P., and Bixby, J.L. (2017). The mTOR Substrate S6 Kinase 1 (S6K1) Is a Negative Regulator of Axon Regeneration and a Potential Drug Target for Central Nervous System Injury. J Neurosci 37, 7079-7095.

Andrews, M.R., Soleman, S., Cheah, M., Tumbarello, D.A., Mason, M.R., Moloney, E., Verhaagen, J., Bensadoun, J.C., Schneider, B., Aebischer, P., and Fawcett, J.W. (2016). Axonal Localization of Integrins in the CNS Is Neuronal Type and Age Dependent. eNeuro 3.

Bilanges, B., Posor, Y., and Vanhaesebroeck, B. (2019). PI3K isoforms in cell signalling and vesicle trafficking. Nat Rev Mol Cell Biol.

Blackmore, M.G., Wang, Z., Lerch, J.K., Motti, D., Zhang, Y.P., Shields, C.B., Lee, J.K., Goldberg, J.L., Lemmon, V.P., and Bixby, J.L. (2012). Kruppel-like Factor 7 engineered for transcriptional activation promotes axon regeneration in the adult corticospinal tract. Proc Natl Acad Sci U S A 109, 7517-7522.

Cheah, M., Andrews, M.R., Chew, D.J., Moloney, E.B., Verhaagen, J., Fassler, R., and Fawcett, J.W. (2016). Expression of an Activated Integrin Promotes Long-Distance Sensory Axon Regeneration in the Spinal Cord. The Journal of neuroscience : the official journal of the Society for Neuroscience 36, 7283-7297.

Cheng, P.L., Song, A.H., Wong, Y.H., Wang, S., Zhang, X., and Poo, M.M. (2011). Self-amplifying autocrine actions of BDNF in axon development. Proceedings of the National Academy of Sciences of the United States of America 108, 18430-18435.

Cosker, K.E., and Eickholt, B.J. (2007). Phosphoinositide 3-kinase signalling events controlling axonal morphogenesis. Biochem Soc Trans 35, 207-210.

Curcio, M., and Bradke, F. (2018). Axon Regeneration in the Central Nervous System: Facing the Challenges from the Inside. Annu Rev Cell Dev Biol 34, 495-521.

De Sousa, P.A., Tye, B.J., Bruce, K., Dand, P., Russell, G., Collins, D.M., Greenshields, A., McDonald, K., Bradburn, H., Allan, D.*, et al.* (2016). Derivation of the clinical grade human embryonic stem cell line RCe021-A (RC-17). Stem Cell Res 17, 1-5.

Duan, X., Qiao, M., Bei, F., Kim, I.J., He, Z., and Sanes, J.R. (2015). Subtype-specific regeneration of retinal ganglion cells following axotomy: effects of osteopontin and mTOR signaling. Neuron 85, 1244-1256.

Eickholt, B.J., Ahmed, A.I., Davies, M., Papakonstanti, E.A., Pearce, W., Starkey, M.L., Bilancio, A., Need, A.C., Smith, A.J., Hall, S.M.*, et al.* (2007). Control of axonal growth and regeneration of sensory neurons by the p110delta PI 3-kinase. PLoS ONE 2, e869.

Eva, R., Dassie, E., Caswell, P.T., Dick, G., ffrench-Constant, C., Norman, J.C., and Fawcett, J.W. (2010). Rab11 and its effector Rab coupling protein contribute to the trafficking of beta 1 integrins during axon growth in adult dorsal root ganglion neurons and PC12 cells. The Journal of neuroscience : the official journal of the Society for Neuroscience 30, 11654-11669.

Eva, R., Koseki, H., Kanamarlapudi, V., and Fawcett, J.W. (2017). EFA6 regulates selective polarised transport and axon regeneration from the axon initial segment. J Cell Sci 130, 3663-3675.

Fagoe, N.D., Attwell, C.L., Kouwenhoven, D., Verhaagen, J., and Mason, M.R. (2015). Overexpression of ATF3 or the combination of ATF3, c-Jun, STAT3 and Smad1 promotes regeneration of the central axon branch of sensory neurons but without synergistic effects. Hum Mol Genet 24, 6788-6800.

Franssen, E.H., Zhao, R.R., Koseki, H., Kanamarlapudi, V., Hoogenraad, C.C., Eva, R., and Fawcett, J.W. (2015). Exclusion of integrins from CNS axons is regulated by Arf6 activation and the AIS. J Neurosci 35, 8359-8375.

Gardiner, N.J., Moffatt, S., Fernyhough, P., Humphries, M.J., Streuli, C.H., and Tomlinson, D.R. (2007). Preconditioning injury-induced neurite outgrowth of adult rat sensory neurons on fibronectin is mediated by mobilisation of axonal alpha5 integrin. Molecular and cellular neurosciences 35, 249-260.

Geoffroy, C.G., Lorenzana, A.O., Kwan, J.P., Lin, K., Ghassemi, O., Ma, A., Xu, N., Creger, D., Liu, K., He, Z., and Zheng, B. (2015). Effects of PTEN and Nogo Codeletion on Corticospinal Axon Sprouting and Regeneration in Mice. The Journal of neuroscience : the official journal of the Society for Neuroscience 35, 6413-6428.

Gibson, D.G., Young, L., Chuang, R.Y., Venter, J.C., Hutchison, C.A., 3rd, and Smith, H.O. (2009). Enzymatic assembly of DNA molecules up to several hundred kilobases. Nat Methods 6, 343-345.

Gillingham, A.K., and Munro, S. (2007). The small G proteins of the Arf family and their regulators. Annu Rev Cell Dev Biol 23, 579-611.

Goldberg, J.L., Klassen, M.P., Hua, Y., and Barres, B.A. (2002). Amacrine-signaled loss of intrinsic axon growth ability by retinal ganglion cells. Science 296, 1860-1864.

Hammond, G.R., Schiavo, G., and Irvine, R.F. (2009). Immunocytochemical techniques reveal multiple, distinct cellular pools of PtdIns4P and PtdIns(4,5)P(2). Biochem J 422, 23-35.

Hawkins, P.T., and Stephens, L.R. (2015). PI3K signalling in inflammation. Biochim Biophys Acta 1851, 882-897.

He, Z., and Jin, Y. (2016). Intrinsic Control of Axon Regeneration. Neuron 90, 437-451.

Henle, S.J., Wang, G., Liang, E., Wu, M., Poo, M.M., and Henley, J.R. (2011). Asymmetric PI(3,4,5)P3 and Akt signaling mediates chemotaxis of axonal growth cones. The Journal of neuroscience : the official journal of the Society for Neuroscience 31, 7016-7027.

Hervera, A., Zhou, L., Palmisano, I., McLachlan, E., Kong, G., Hutson, T.H., Danzi, M.C., Lemmon, V.P., Bixby, J.L., Matamoros-Angles, A., *et al.* (2019). PP4-dependent HDAC3 dephosphorylation discriminates between axonal regeneration and regenerative failure. EMBO J.

Hollis, E.R., 2nd, Jamshidi, P., Low, K., Blesch, A., and Tuszynski, M.H. (2009a). Induction of corticospinal regeneration by lentiviral trkB-induced Erk activation. Proceedings of the National Academy of Sciences of the United States of America 106, 7215-7220.

Hollis, E.R., 2nd, Lu, P., Blesch, A., and Tuszynski, M.H. (2009b). IGF-I gene delivery promotes corticospinal neuronal survival but not regeneration after adult CNS injury. Exp Neurol 215, 53-59.

Hu, Y., Poopalasundaram, S., Graham, A., and Bouloux, P.M. (2013). GnRH neuronal migration and olfactory bulb neurite outgrowth are dependent on FGF receptor 1 signaling, specifically via the PI3K p110alpha isoform in chick embryo. Endocrinology 154, 388-399.

Kakumoto, T., and Nakata, T. (2013). Optogenetic control of PIP3: PIP3 is sufficient to induce the actin-based active part of growth cones and is regulated via endocytosis. PLoS One 8, e70861.

Kalil, K., and Reh, T. (1979). Regrowth of severed axons in the neonatal central nervous system: establishment of normal connections. Science 205, 1158-1161.

Kang, S., Denley, A., Vanhaesebroeck, B., and Vogt, P.K. (2006). Oncogenic transformation induced by the p110beta, -gamma, and -delta isoforms of class I phosphoinositide 3-kinase. Proc Natl Acad Sci U S A 103, 1289-1294.

Kath, C., Goni-Oliver, P., Muller, R., Schultz, C., Haucke, V., Eickholt, B., and Schmoranzer, J. (2018). PTEN suppresses axon outgrowth by down-regulating the level of detyrosinated microtubules. PLoS One 13, e0193257.

Koseki, H., Donegá, M., Lam, B.Y.H., Petrova, V., van Erp, S., Yeo, G.S.H., Kwok, J.C.F., ffrench-Constant, C., Eva, R., and Fawcett, J. (2017). Selective Rab11 transport and the intrinsic regenerative ability of CNS axons. Elife 6, e26956.

Kreis, P., Leondaritis, G., Lieberam, I., and Eickholt, B.J. (2014). Subcellular targeting and dynamic regulation of PTEN: implications for neuronal cells and neurological disorders. Front Mol Neurosci 7, 23.

Lindsay, A.J., and McCaffrey, M.W. (2004). The C2 domains of the class I Rab11 family of interacting proteins target recycling vesicles to the plasma membrane. Journal of cell science 117, 4365-4375.

Liu, K., Lu, Y., Lee, J.K., Samara, R., Willenberg, R., Sears-Kraxberger, I., Tedeschi, A., Park, K.K., Jin, D., Cai, B., *et al.* (2010). PTEN deletion enhances the regenerative ability of adult corticospinal neurons. Nature neuroscience 13, 1075-1081.

Liu, Y., Wang, X., Li, W., Zhang, Q., Li, Y., Zhang, Z., Zhu, J., Chen, B., Williams, P.R., Zhang, Y., *et al.* (2017). A Sensitized IGF1 Treatment Restores Corticospinal Axon-Dependent Functions. Neuron 95, 817-833 e814.

Longair, M.H., Baker, D.A., and Armstrong, J.D. (2011). Simple Neurite Tracer: open source software for reconstruction, visualization and analysis of neuronal processes. Bioinformatics 27, 2453-2454.

Low, P.C., Manzanero, S., Mohannak, N., Narayana, V.K., Nguyen, T.H., Kvaskoff, D., Brennan, F.H., Ruitenberg, M.J., Gelderblom, M., Magnus, T., *et al.* (2014). PI3Kdelta inhibition reduces TNF secretion and neuroinflammation in a mouse cerebral stroke model. Nat Commun 5, 3450.

Luikart, B.W., Schnell, E., Washburn, E.K., Bensen, A.L., Tovar, K.R., and Westbrook, G.L. (2011). Pten knockdown in vivo increases excitatory drive onto dentate granule cells. J Neurosci 31, 4345-4354.

Malek, M., Kielkowska, A., Chessa, T., Anderson, K.E., Barneda, D., Pir, P., Nakanishi, H., Eguchi, S., Koizumi, A., Sasaki, J., *et al.* (2017). PTEN Regulates PI(3,4)P2 Signaling Downstream of Class I PI3K. Mol Cell 68, 566-580 e510.

Mandelker, D., Gabelli, S.B., Schmidt-Kittler, O., Zhu, J., Cheong, I., Huang, C.H., Kinzler, K.W., Vogelstein, B., and Amzel, L.M. (2009). A frequent kinase domain mutation that changes the interaction between PI3Kalpha and the membrane. Proc Natl Acad Sci U S A 106, 16996-17001.

Martinez-Marmol, R., Mohannak, N., Qian, L., Wang, T., Gormal, R.S., Ruitenberg, M.J., Vanhaesebroeck, B., Coulson, E.J., and Meunier, F.A. (2019). p110delta PI 3-kinase inhibition perturbs APP and TNFalpha trafficking, reduces plaque burden, dampens neuroinflammation and prevents cognitive decline in an Alzheimer's disease mouse model. J Neurosci.

Menager, C., Arimura, N., Fukata, Y., and Kaibuchi, K. (2004). PIP3 is involved in neuronal polarization and axon formation. Journal of neurochemistry 89, 109-118.

Ming, G., Song, H., Berninger, B., Inagaki, N., Tessier-Lavigne, M., and Poo, M. (1999). Phospholipase C-gamma and phosphoinositide 3-kinase mediate cytoplasmic signaling in nerve growth cone guidance. Neuron 23, 139-148.

Nieuwenhuis, B., and Eva, R. (2018). ARF6 and Rab11 as intrinsic regulators of axon regeneration. Small Gtpases, 1-10.

Nishio, M., Watanabe, K., Sasaki, J., Taya, C., Takasuga, S., Iizuka, R., Balla, T., Yamazaki, M., Watanabe, H., Itoh, R., *et al.* (2007). Control of cell polarity and motility by the PtdIns(3,4,5)P3 phosphatase SHIP1. Nat Cell Biol 9, 36-44.

Nyabi, O., Naessens, M., Haigh, K., Gembarska, A., Goossens, S., Maetens, M., De Clercq, S., Drogat, B., Haenebalcke, L., Bartunkova, S., *et al.* (2009). Efficient mouse transgenesis using Gateway-compatible ROSA26 locus targeting vectors and F1 hybrid ES cells. Nucleic Acids Res 37, e55.

Okkenhaug, K. (2013). Signaling by the phosphoinositide 3-kinase family in immune cells. Annu Rev Immunol 31, 675-704.

Park, K.K., Liu, K., Hu, Y., Smith, P.D., Wang, C., Cai, B., Xu, B., Connolly, L., Kramvis, I., Sahin, M., and He, Z. (2008). Promoting axon regeneration in the adult CNS by modulation of the PTEN/mTOR pathway. Science 322, 963-966.

Petrova, V., and Eva, R. (2018). The virtuous cycle of axon growth: Axonal transport of growth-promoting machinery as an intrinsic determinant of axon regeneration. Dev Neurobiol.

Poulopoulos, A., Murphy, A.J., Ozkan, A., Davis, P., Hatch, J., Kirchner, R., and Macklis, J.D. (2019). Subcellular transcriptomes and proteomes of developing axon projections in the cerebral cortex. Nature 565, 356-360.

Puttagunta, R., Tedeschi, A., Soria, M.G., Hervera, A., Lindner, R., Rathore, K.I., Gaub, P., Joshi, Y., Nguyen, T., Schmandke, A., *et al.* (2014). PCAF-dependent epigenetic changes promote axonal regeneration in the central nervous system. Nat Commun 5, 3527.

Richardson, P.M., Issa, V.M., and Aguayo, A.J. (1984). Regeneration of long spinal axons in the rat. J Neurocytol 13, 165-182.

Richardson, P.M., Miao, T., Wu, D., Zhang, Y., Yeh, J., and Bo, X. (2009). Responses of the nerve cell body to axotomy. Neurosurgery 65, A74-79.

Samuels, Y., Wang, Z., Bardelli, A., Silliman, N., Ptak, J., Szabo, S., Yan, H., Gazdar, A., Powell, S.M., Riggins, G.J., *et al.* (2004). High frequency of mutations of the PIK3CA gene in human cancers. Science 304, 554.

Schmitz, S.K., Hjorth, J.J., Joemai, R.M., Wijntjes, R., Eijgenraam, S., de Bruijn, P., Georgiou, C., de Jong, A.P., van Ooyen, A., Verhage, M., *et al.* (2011). Automated analysis of neuronal morphology, synapse number and synaptic recruitment. J Neurosci Methods 195, 185-193.

Shi, S.H., Jan, L.Y., and Jan, Y.N. (2003). Hippocampal neuronal polarity specified by spatially localized mPar3/mPar6 and PI 3-kinase activity. Cell 112, 63-75.

Smith, D.S., and Skene, J.H. (1997). A transcription-dependent switch controls competence of adult neurons for distinct modes of axon growth. J Neurosci 17, 646-658.

Smith, P.D., Sun, F., Park, K.K., Cai, B., Wang, C., Kuwako, K., Martinez-Carrasco, I., Connolly, L., and He, Z. (2009). SOCS3 deletion promotes optic nerve regeneration in vivo. Neuron 64, 617-623.

Sosa, L., Dupraz, S., Laurino, L., Bollati, F., Bisbal, M., Caceres, A., Pfenninger, K.H., and Quiroga, S. (2006). IGF-1 receptor is essential for the establishment of hippocampal neuronal polarity. Nat Neurosci 9, 993-995.

Tedeschi, A., and Bradke, F. (2017). Spatial and temporal arrangement of neuronal intrinsic and extrinsic mechanisms controlling axon regeneration. Curr Opin Neurobiol 42, 118-127.

Tedeschi, A., Dupraz, S., Laskowski, C.J., Xue, J., Ulas, T., Beyer, M., Schultze, J.L., and Bradke, F. (2016). The Calcium Channel Subunit Alpha2delta2 Suppresses Axon Regeneration in the Adult CNS. Neuron 92, 419-434.

Tsujita, K., and Itoh, T. (2015). Phosphoinositides in the regulation of actin cortex and cell migration. Biochim Biophys Acta 1851, 824-831.

Varnai, P., Bondeva, T., Tamas, P., Toth, B., Buday, L., Hunyady, L., and Balla, T. (2005). Selective cellular effects of overexpressed pleckstrin-homology domains that recognize PtdIns(3,4,5)P3 suggest their interaction with protein binding partners. J Cell Sci 118, 4879-4888.

Welch, H.C., Coadwell, W.J., Ellson, C.D., Ferguson, G.J., Andrews, S.R., Erdjument-Bromage, H., Tempst, P., Hawkins, P.T., and Stephens, L.R. (2002). P-Rex1, a PtdIns(3,4,5)P3- and Gbetagamma-regulated guanine-nucleotide exchange factor for Rac. Cell 108, 809-821.

Weng, Y.L., Wang, X., An, R., Cassin, J., Vissers, C., Liu, Y., Liu, Y., Xu, T., Wang, X., Wong, S.Z.H., *et al.* (2018). Epitranscriptomic m(6)A Regulation of Axon Regeneration in the Adult Mammalian Nervous System. Neuron 97, 313-325 e316.

Willenberg, R., Zukor, K., Liu, K., He, Z., and Steward, O. (2016). Variable laterality of corticospinal tract axons that regenerate after spinal cord injury as a result of PTEN deletion or knock-down. J Comp Neurol 524, 2654-2676.

Wu, Z., Ghosh-Roy, A., Yanik, M.F., Zhang, J.Z., Jin, Y., and Chisholm, A.D. (2007). Caenorhabditis elegans neuronal regeneration is influenced by life stage, ephrin signaling, and synaptic branching. Proc Natl Acad Sci U S A 104, 15132-15137.

Xin, L., Lawson, D.A., and Witte, O.N. (2005). The Sca-1 cell surface marker enriches for a prostate-regenerating cell subpopulation that can initiate prostate tumorigenesis. Proc Natl Acad Sci U S A 102, 6942-6947.

Ylera, B., Erturk, A., Hellal, F., Nadrigny, F., Hurtado, A., Tahirovic, S., Oudega, M., Kirchhoff, F., and Bradke, F. (2009). Chronically CNS-injured adult sensory neurons gain regenerative competence upon a lesion of their peripheral axon. Curr Biol 19, 930-936.

Yoshizawa, M., Kawauchi, T., Sone, M., Nishimura, Y.V., Terao, M., Chihama, K., Nabeshima, Y., and Hoshino, M. (2005). Involvement of a Rac activator,P-Rex1, in neurotrophin-derived signaling and neuronal migration. J Neurosci 25, 4406-4419.

Yungher, B.J., Luo, X., Salgueiro, Y., Blackmore, M.G., and Park, K.K. (2015). Viral vector-based improvement of optic nerve regeneration: characterization of individual axons' growth patterns and synaptogenesis in a visual target. Gene Ther 22, 811-821.

Zhang, Y., Chen, K., Sloan, S.A., Bennett, M.L., Scholze, A.R., O'Keeffe, S., Phatnani, H.P., Guarnieri, P., Caneda, C., Ruderisch, N., *et al.* (2014). An RNA-sequencing transcriptome and splicing database of glia, neurons, and vascular cells of the cerebral cortex. J Neurosci 34, 11929-11947.

Zhang, Y., Sloan, S.A., Clarke, L.E., Caneda, C., Plaza, C.A., Blumenthal, P.D., Vogel, H., Steinberg, G.K., Edwards, M.S., Li, G., *et al.* (2016). Purification and Characterization of Progenitor and Mature Human Astrocytes Reveals Transcriptional and Functional Differences with Mouse. Neuron 89, 37-53.

Zhang, Y., Williams, P.R., Jacobi, A., Wang, C., Goel, A., Hirano, A.A., Brecha, N.C., Kerschensteiner, D., and He, Z. (2019). Elevating Growth Factor Responsiveness and Axon Regeneration by Modulating Presynaptic Inputs. Neuron.

Zhao, J.J., Liu, Z., Wang, L., Shin, E., Loda, M.F., and Roberts, T.M. (2005). The oncogenic properties of mutant p110alpha and p110beta phosphatidylinositol 3-kinases in human mammary epithelial cells. Proc Natl Acad Sci U S A 102, 18443-18448.

Zhou, F.Q., Zhou, J., Dedhar, S., Wu, Y.H., and Snider, W.D. (2004). NGF-induced axon growth is mediated by localized inactivation of GSK-3beta and functions of the microtubule plus end binding protein APC. Neuron 42, 897-912.

Zukor, K., Belin, S., Wang, C., Keelan, N., Wang, X., and He, Z. (2013). Short hairpin RNA against PTEN enhances regenerative growth of corticospinal tract axons after spinal cord injury. J Neurosci 33, 15350-15361.